

CHAPTER-IV

Section A

Green Synthesis of 3,4-dihydropyrimidine-2-(1H)-ones (DHPMs) using Iron Borate as an Efficient Catalyst

4.A.1 Background of the present investigation

In synthetic organic chemistry, it is becoming increasingly important to develop clean and environmentally sound chemical processes that use less hazardous reaction conditions and covers the essential prospects of green chemistry principle. Solvent free reaction on one hand provides avenues for the requirement of green chemical condition as this reaction condition are highly significant from both the economic and environmental point of view¹. Now a days, one-pot Multicomponent Reactions are gaining lot of interest for the synthesis of wide range of biologically active heterocyclic compounds². Thus, the combination of solvent free reaction condition and one-pot Multicomponent reaction could serve as an optimal and efficient method for the synthesis of diverse class of heterocyclic compounds under green chemical conditions. Since this type of combination has many added advantages such as short reaction time, economical, environmentally benign, elimination of hazardous solvents and easy work up procedure over the classical synthetic methods³. Among the numerous Multicomponent reactions, Bigenelli reaction is used for the direct synthesis of 3,4-dihydropyrimidine-2-(1H)-one derivatives. The Bigenelli Reaction coined by Italian Chemist Pietro Bigenelli in 1893 is one of the most important and useful multicomponent condensation reaction involving an aldehyde, urea and β -dicarbonyl compounds to yield 3,4-dihydropyrimidine-2-(1H)-ones (Fig. 4.A.1a). These compounds are somewhat similar to dihydropyridines also known as Hantzsch pyridines as the preparation of these compounds also requires the same reactants as required for preparation of Bigenelli compounds⁴. The reaction can also be carried out by using thiourea in place of urea to yield 3,4-dihydropyrimidine-2-(1H)-thione (Fig. 4. A.1b)⁵. In recent times, DHPMs have gained a lot of attention of chemists because of their biological and therapeutic uses⁶. These compounds are one among the five classes of Calcium Channel blocking drugs⁷⁻⁸. They also have anti-viral⁹, anti-inflammatory, anti-bacterial¹⁰, α -1a-adrenergic antagonist¹¹, anti-tumor¹², anti-cancer¹³, anti-HIV¹⁴, anti-inflammatory¹⁵ properties. Apart from these properties, DHPMs also have shown other significant properties like anti-oxidant¹⁶, antimuscarinic¹⁷, antithyroid¹⁸, antiparasitic¹⁹, antidiabetic²⁰, Urease Inhibition²¹, Carbonic anhydrase inhibition²², cardiac effects²³. DHPMs are also present in some polyguanidine alkaloids like batzelladine that have found been found to be HIV gp-120-CD-4 inhibitors²⁴. Few important drugs that contain the DHPM moiety are monastrol (99), riboflavin (100), 5-Fluoro uracil (101), aminophylline (102), idoxuridine (103) Fig.4. A.2.

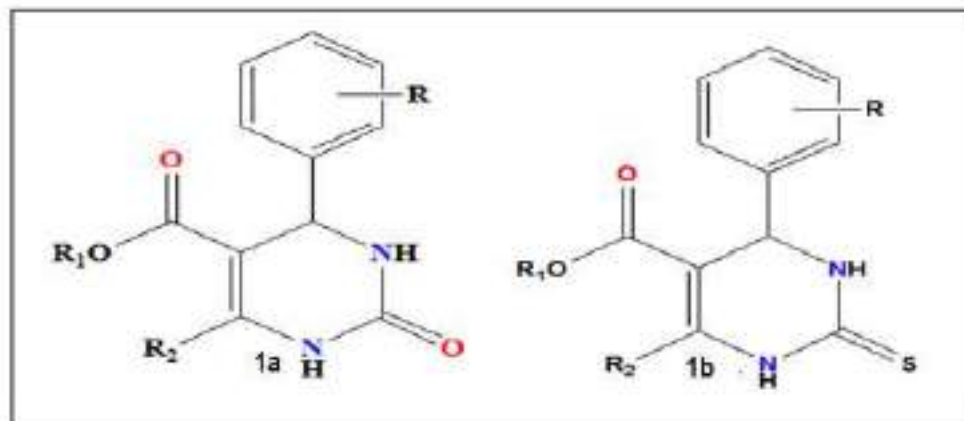


Fig. 4.A.1a-1b. 1a) Structure of yield 3,4-dihydropyrimidine-2-(1H)-one and 1b) 3,4-dihydropyrimidine-2-(1H)-thione

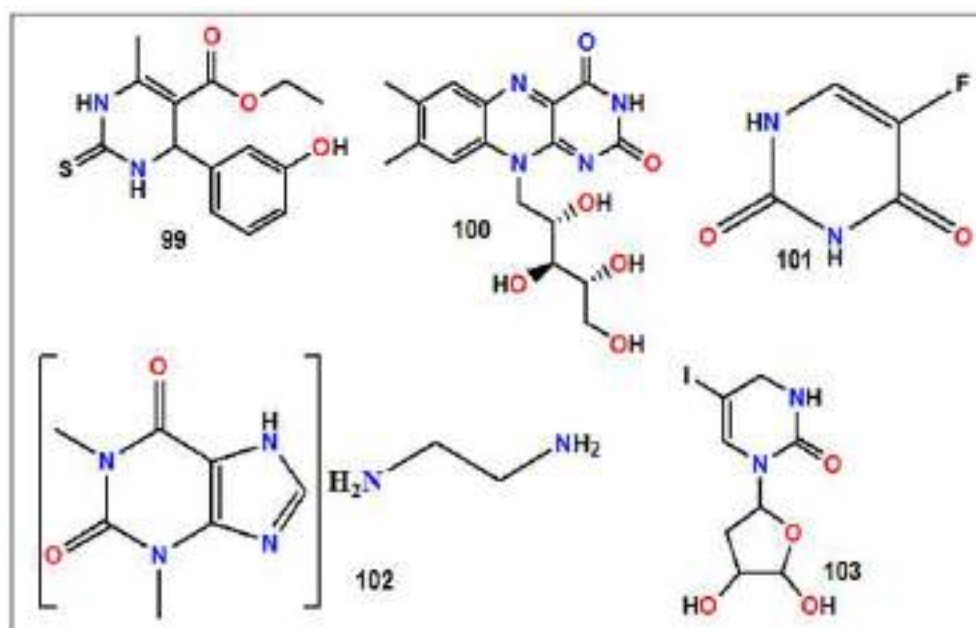


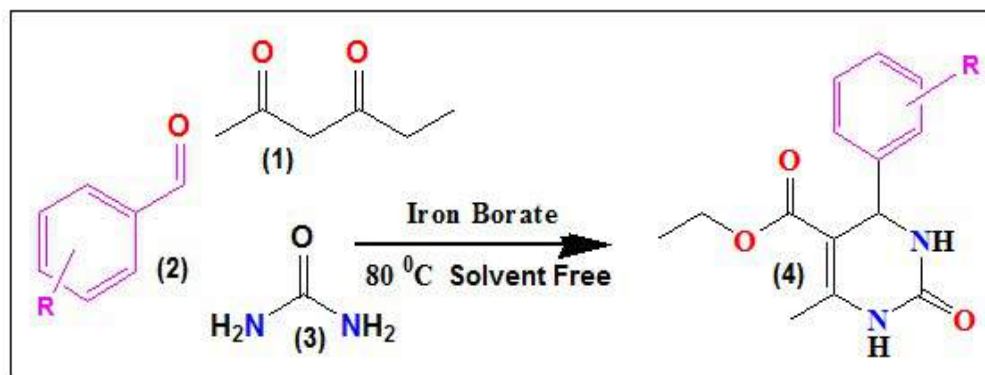
Fig. 4.A.2. Structures of few drugs that contain the DHPM moiety

In view of the diverse pharmacological, medicinal, biological and industrial properties associated with 3, 4-dihydropyrimidine derivatives, numerous synthetic methodologies have been developed during the past few decades under both classical and green chemical conditions²⁵⁻²⁶. However, these reported synthetic procedures found to contain one or more serious drawbacks such as use of expensive catalyst, non-recyclable catalyst, moisture sensitive metal salts, long reaction time, low yield, large amount of catalyst loading, use of hazardous solvent, tedious work-up procedure and environmental pollution²⁷. Thus, the development of a clean, environmentally benign and economically cost-effective

protocol for the synthesis of 3, 4-dihydropyrimidine-2-(1H)-one derivatives is highly demanding and, in this context, synthetic chemists are devoting time to develop a protocol for solvent free synthesis, solid phase synthesis and even reaction in water medium. The prominent advantages of solvent free, solid phase or reaction in water medium is that it omits the use of the environmentally hazardous solvents which definitely reduce chemical pollution and at the same time reduce the cost of the work²⁸. Therefore, in order to overcome these shortcomings and fulfilling the criteria of green chemistry principle and sustainable chemistry, in this chapter, we are reporting the synthesis of 3, 4-dihydropyrimidine-2-(1H)-one derivatives using inexpensive iron borate as a catalyst under solvent free condition.

4.A.2. Results and Discussions

The classical method for the synthesis of 3,4-dihydropyrimidine-2-ones (4) involves a one pot condensation of β -keto ester (1), aldehyde (2) and urea (3) under harsh acidic conditions with low yield of the products²⁹. Thus, it has become inevitable that the synthesis of 3, 4-dihydropyrimidine-2-ones to be pursued in an environmentally friendly manner for its use in different fields³⁰. Although a large variety of new catalytic / modified synthetic protocols such as microwave assisted, Ultrasound irradiation, use of ionic liquid, solvent free synthesis has been developed for the synthesis of 3, 4-dihydropyrimidine-2-one derivatives in an elegant manner during the past few decades yet these reported protocols encounter some serious limitations as discussed above³¹⁻⁴⁰. These factors prompted us to find a new catalyst for the synthesis of Bigenelli derivatives under solvent free condition. A number of reports are available for the synthesis of 3, 4-dihydropyrimidine-2-one derivatives using different iron salts as a catalyst under different reaction condition but there is not a single report for the synthesis of the above mention derivatives using iron borate as a catalyst. Therefore, it was thought worthwhile to explore the catalytic efficacy of iron borate for the synthesis of 3, 4-dihydropyrimidine-2-one derivatives (4) by one-pot cyclo-condensation of β -dicarbonyl compound (1), Aldehyde (2) and Urea (3) under solvent free reaction condition following the green chemistry protocol (Scheme 4.A.1).



Scheme. 4.A.1. Schematic representation of Biginelli reaction catalyzed by Fe-borate catalyst

Initially, for the synthesis 3, 4-dihydropyrimidine-2-ones (4), we choose ethylacetoacetate (1), 2-nitrobenzaldehyde (2) and urea (3) as model compounds under different environmentally friendly reaction conditions at 80 °C for 3 hours using different mol% (0.5 to 4) of the catalyst iron borate. We choose the different solvent systems as well for screening the catalytic efficiency of the catalyst with model reactants under different conditions and the results are summarized in Table 4.A.1

Table. 4.A.1. Screening of the solvent for control reaction

Entry	Solvent ^a	Time (hours)	Yield ^b
1	Ethanol	3	86
2	Methanol	3	82
3	DMF	3	90
4	DMSO	3	80
5	Water	3	40
6	Silica Gel	1	86
7	Neat	8 (mins)	97

^aThe reaction was performed with Ethylacetoacetate 1(1 mmol), 2-nitro-Benzaldehyde 2 (1 mmol), and Urea 3 (1 mmol) with the catalyst using different solvents. ^bIsolated Yields.

We observed that the Biginelli reaction proceed well in more polar solvent like alcohol, DMF and DMSO (Table 4.A.1, entry 1, 2, 3, 4) but we observed that under this condition, the reaction needed more time to go for completion. Therefore, we focused our study towards the green protocol employing solid phase

synthesis using silica gel as a reaction medium but in this case also we found that under this condition, the work-up of the desired product needs more attention and rigorous techniques such as column chromatography to recover the final product (Table 4.A.1, entry 6).

Therefore, these limitations prompted us to investigate more suitable and environmentally friendly reaction condition for the synthesis of 3, 4-dihydropyrimidine-2-ones (4). As a part of the green chemical methodology, we were interested to carry out the above reaction under solvent free condition and encouragingly we encountered that the desired product formed with good yield and less reaction time (6-8 minutes) (Table 4.A.1, entry 7). The results of the model reaction for different mol% of the catalyst loading under optimized condition are listed in Table 4.A.2.

Table 4.A.2. Screening of the amount of the catalyst for the model reaction

Entry	Catalyst mol % ^a	Temperature (^o C)	Time (Minutes)	Yield ^b (%)
1	0	80	8	15
2	0.5	80	8	65
3	1.0	80	8	70
4	1.5	80	8	73
5	2.0	80	8	80
6	2.5	80	8	91
7	3.0	80	8	97
8	3.5	80	8	94
9	4.0	80	8	94

^aThe reaction was performed with Ethyl acetoacetate 1 (1 mmol) 2-nitrobenzaldehyde 2 (1 mmol), and Urea 3 (1 mmol) with the catalyst under solvent free condition. ^bIsolated Yields.

Interestingly, we observed that the reaction proceeds in much faster rate under solvent free condition in short reaction time (8 minutes) when the amount of catalyst loading is 3 mol% (Table 4.A.2, entry 7). A controlled reaction without catalyst leads to the formation of the product in negligible amount (Table 4.A.2, entry 1). Having recognized the optimal reaction condition, we subsequently examined the catalytic efficiency and applicability of this protocol by extending this protocol with differently substituted aldehydes (2) and keeping the component (1) and (3) fixed (Fig. tt). We examined that all the reactions proceeded well and smoothly in very short reaction time to afford the desired products, 3,4-

dihydropyrimidine-2-ones (4a-r) in good to excellent yields (90-98%) (Fig 4.A.3 and Table 4.A.3).

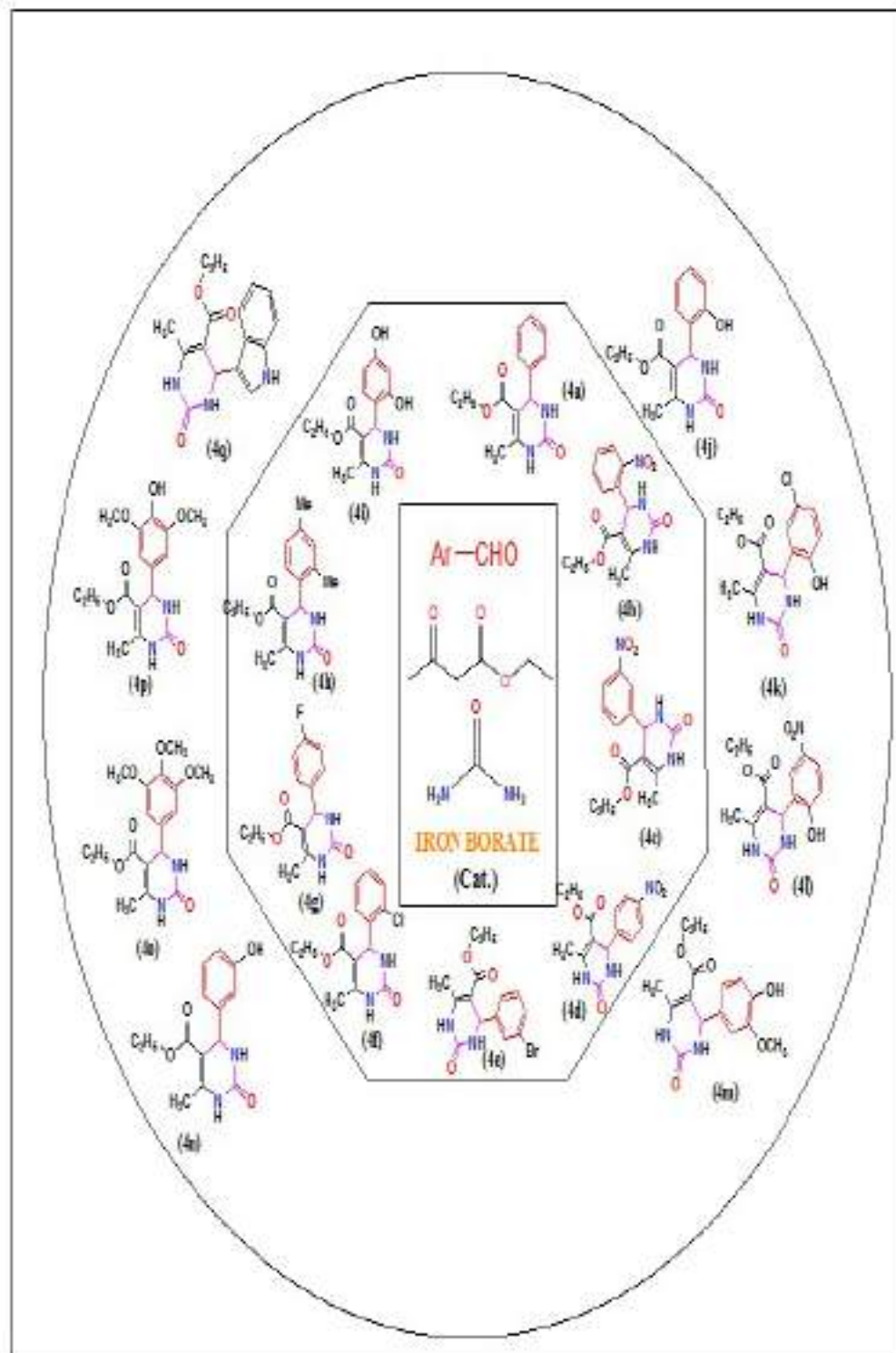


Fig. 4.A.3. Pictorial representation of the Biginelli products (4a-4q).

Table. 4.A.3. Iron Borate catalyzed solvent free neat synthesis of 3,4-dihydropyrimidine-2-one derivatives (4a-4q)

Entry	B-keto ester	Aldehyde substrate	Product	Yield ^b (%)
1	Ethylacetoacetate	Benzaldehyde	4a	97
2	Ethylacetoacetate	2-nitrobenzaldehyde	4b	98
3	Ethylacetoacetate	3-nitrobenzaldehyde	4c	97
4	Ethylacetoacetate	4-nitrobenzaldehyde	4d	96
5	Ethylacetoacetate	3-bromobenzaldehyde	4e	96
6	Ethylacetoacetate	2-chlorobenzaldehyde	4f	97
7	Ethylacetoacetate	4-fluorobenzaldehyde	4g	97
8	Ethylacetoacetate	2,4-dimethylbenzaldehyde	4h	93
9	Ethylacetoacetate	2,4-dihydroxybenzaldehyde	4i	92
10	Ethylacetoacetate	2-hydroxybenzaldehyde	4j	95
11	Ethylacetoacetate	5-chloro-2-hydroxybenzaldehyde	4k	96
12	Ethylacetoacetate	5-nitro-2-hydroxybenzaldehyde	4l	95
13	Ethylacetoacetate	4-hydroxy-3-methoxybenzaldehyde	4m	88
14	Ethylacetoacetate	3-hydroxybenzaldehyde	4n	90
15	Ethylacetoacetate	3,4,5-trimethoxybenzaldehyde	4o	88
16	Ethylacetoacetate	4-hydroxy-3, 5-dimethoxybenzaldehyde	4p	88
16	Ethylacetoacetate	Indole-3-carboxaldehyde	4q	90

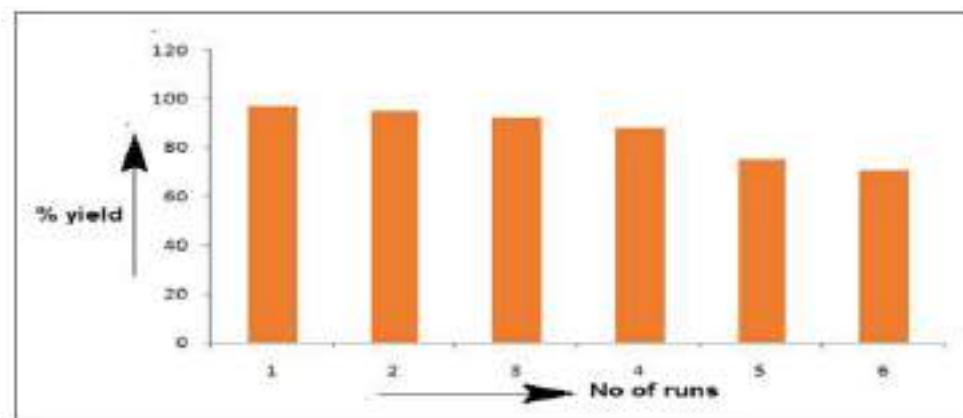
^bIsolated yields

Moreover, it is interesting to note that para-substituted benzaldehyde with electron withdrawing group successfully afforded the corresponding product in excellent yield under optimized condition as compared to the electron releasing group present at the same position. Ortho and meta-substituted aldehydes also afforded the desired products in good yields but they required more time for reaction to complete.

We then compared the catalytic efficacy of the iron borate with different catalyst reported in the literature documented elsewhere and we found that iron borate has high catalytic efficiency and recyclability as compared to other catalyst and needs only few minutes for the completion of the reaction. Surprisingly, we could recover the catalyst after 4th run also and we observed that the catalyst lost its efficiency partially after 5th run of the reaction (Table 4.A.4).

Table 4.A.4. Study on the recyclability of the catalyst

Entry	No. of runs	Isolated yields (%)
1	1	97
2	2	95
3	3	92
4	4	88
5	5	75
6	6	71

**Fig. 4.A.4.** Recyclability of the catalyst

It was observed during the reaction that a variety of functional groups like acidic, nitro, methoxy, etc. remains un-affected during the reaction. Substituted benzaldehydes with either electron donating or electron withdrawing groups afforded good yield of the products, however it was also found that benzaldehyde with electron releasing groups gave a slight less yield of the products. We also compared the catalytic efficiency of Iron borate with other previously reported catalysts and found that Iron Borate has high catalytic efficiency and required less reaction time to go for completion Table 4.A.5.

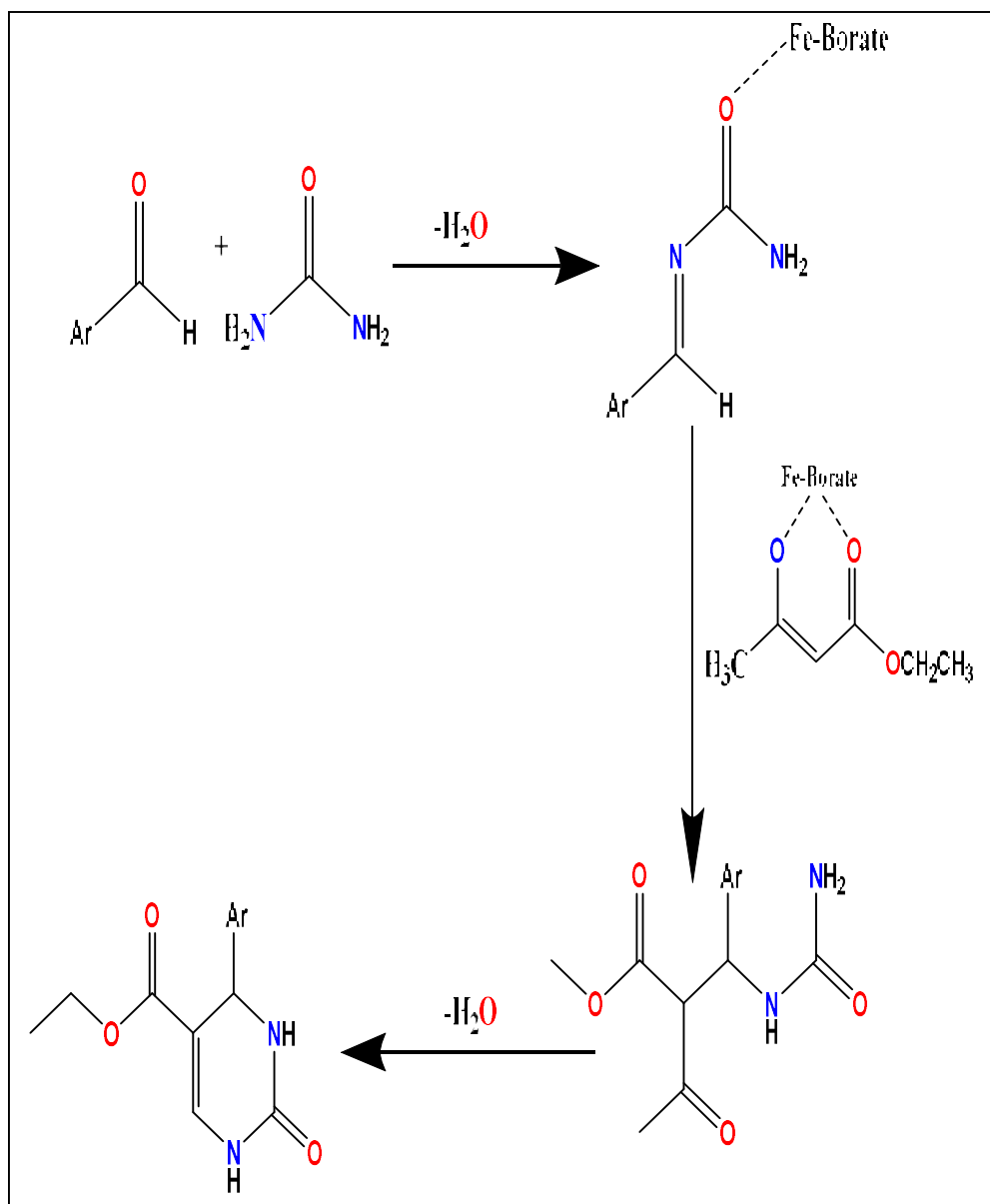
Table. 4.A.5. Comparison of Catalytic efficiency of Iron Borate with other reported catalysts for the synthesis of 3,4-dihydropyrimidine-2-one derivatives (4a-4q).

Entry	Catalyst	Solvent ^a	Temperature	Time	Yield (%) ^b
1	IL-OPPh ₂	Neat	100 °C	2.5 hours	91[lit ⁴¹]
2	TSIL	Water	Room Temperature	10 minutes	94[lit ³⁵]
3	[Btto][p-TSA]	Neat	90 °C	30 minutes	96[lit ⁴²]
4	L-Proline nitrate	MeCN	Room Temperature	50 minutes	92[lit ⁴³]
5	Co-functionalised Na ⁺ montmocillonite	Neat	100 °C	10 minutes	92[lit ⁴⁴]
6	BF ₃ .OEt ₂ /CuCl	THF	Reflux	18 hours	71[lit ⁴⁵]
7	Cu(Otf) ₂	EtOH	M.W	1 hour	95[lit ⁴⁶]
8	Chiral-phosphoric acid	DCM	25 °C	4 days	77[lit ⁴⁷]
9	SnCl ₂ -nano SiO ₂	EtOH	Reflux	40 minutes	92[lit ⁴⁸]
10	CD-SO ₃ H	Neat	80 °C	2 hours	89[lit ⁴⁹]
11	Sulfated-Tungstate	Neat	80 °C	1 hour	92[lit ⁵⁰]
12	IRMOF-3	Neat	Reflux	5 hours	89[lit ⁵¹]
13	CsF-Celite	Neat	80 °C	1 hour	95[lit ⁵²]
14	Cuttlebone	Neat	90 °C	10 minutes	92[lit ⁵³]
15	Co(NO ₃) ₂ .6H ₂ O	Neat	80 °C	40 minutes	90[lit ⁵⁴]
16	Iron Borate	Neat	80 °C	8 minutes	97 [This work]

^aComparison of catalytic efficiency of Iron Borate with other reported catalyst for the synthesis of 3,4-dihydropyrimidine-2-one derivatives using benzaldehyde, ethyl acetoacetate and Urea under different reaction conditions. ^bIsolated Yields.

4.A.3 Plausible Mechanism

The Biginelli reaction may proceed through acylimine intermediate (5) which is formed by the imine reaction between an aldehyde (2) and urea (3) catalyzed by iron borate. Further, addition of enolate of β keto-ester (1) to acylimine intermediate followed by dehydration and cyclization leads to the formation of corresponding dihydropyrimidinone derivative (4). A proposed mechanism for the synthesis of 3, 4-dihydropyrimidine-2-one catalyzed by Fe-borate is depicted below in Scheme 4.A.2.



Scheme. 4.A.2. Proposed mechanism for the synthesis of 3, 4-dihydropyrimidine-2-one catalyzed by Fe-borate

4.A.4 Experimental Section

4.A.4.1 Materials

All starting materials of high purity for the described synthesis were purchased commercially as received. The FT-IR spectra of the prepared compounds were recorded in Bruker Alpha III spectrophotometer operating in the wave number region 4000 to 400 cm^{-1} in dry KBr. The melting points of the synthesized compounds were determined by open capillary method. $^1\text{H-NMR}$ spectra of the synthesized 3,4-dihydropyrimidine-2-one derivatives (4a-4u) were recorded at room temperature on a FT-NMR (Bruker Advance-II 400 MHz) spectrometer by using DMSO-d_6 as solvents and chemical shifts are quoted in ppm downfield of internal standard tetramethylsilane(TMS).

4.A.4.2 General procedure for the synthesis of 3,4-dihydropyrimidine-2-ones:

In a typical procedure, a mixture of substituted benzaldehyde (1.0 mmol), ethylacetoacetate (1.0 mmol), urea (1.0 mmol) and Iron borate (3 mol %) thoroughly ground and mixed in a mortar and pestle to make a homogenous mixture. The mixture was then transferred to a test tube. The reaction was heated at 80°C for 8 minutes. The progress of the reaction was monitored by TLC using hexane/ethyl acetate (80:20) solvent. After completion of the reaction, the reaction mixture was dissolved in methanol and filtered. The filtrate was evaporated under vacuum and subsequently dried to afford desired product. All the synthesized compounds (4a-4q) were recrystallized from ethanol and have been characterized by their analytical (yield and melting point value) and spectroscopic data (FT-IR and $^1\text{HNMR}$) and compared with the literature value.

4.A.5. Conclusion

In this chapter, we described a simple, green and efficient procedure for the synthesis of 3,4- dihydropyrimidine-2-one derivatives using an unconventional Iron borate catalyst under solvent free condition. The reaction provides a method for the synthesis of a variety of 3, 4-dihydropyrimidine-2-ones with good to excellent yields and the catalyst has been versatile for a wide range of aromatic aldehydes.

4.A.6. Analytical and Spectroscopic data

4.A.6.1 Ethyl 1,2,3,4-tetrahydro-6-methyl-2-oxo-4-phenylpyrimidine-5-carboxylate (4a): white solid, yield= 97 %, melting point found ($^{\circ}\text{C}$) = 202-205, IR (cm^{-1}) ν_{max} : IR (cm^{-1}) ν_{max} : 3442, 3298, 3190, 2981, (N-H), 1685, 1651 (C=O), ^1H NMR (400 MHz, DMSO d_6): δ_{ppm} = 9.36 (s, 1H, NH), 7.54 (s, 1H, NH), 7.31-7.43 (m, 3H, Ar-H), 5.66 (d, 1H), 3.46 (m, 2H, CH_2), 2.50 (s, 3H, CH_3), 1.07 (t, 3H, CH_3).

4.A.6.2 Ethyl 1,2,3,4-tetrahydro-6-methyl-4-(2-nitrophenyl)-2-oxopyrimidine-5-carboxylate (4b): yellow powder, yield= 98 %, melting point found ($^{\circ}\text{C}$) = 219-221, IR (KBr, cm^{-1}) ν_{max} : 3443, 3369, 3235 (NH), 1685, 1636 cm^{-1} (C=O), ^1H NMR (400 MHz, DMSO- d_6): δ_{ppm} = 9.92 (s, 1H, NH), 8.32 (s, 1H, NH), 7.51 (d, 1H, Ar-H), 7.23-7.27(m, 3H, Ar-H), 5.41 (s, 1H, CH), 4.51(q, 2H, CH_2 of ethyl), 2.49(s, 3H, CH_3), 1.31(t, 3H, CH_3).

4.A.6.3 Ethyl 1,2,3,4-tetrahydro-6-methyl-4-(3-nitrophenyl)-2-oxopyrimidine-5-carboxylate (4c): yellow solid, yield= 97 %, melting point found ($^{\circ}\text{C}$) = 226-229, IR (cm^{-1}) ν_{max} : 3444, 3100, 2985 (NH), 1655, 1532 (C=O), ^1H NMR (400 MHz, DMSO d_6): δ_{ppm} = 9.39 (s, 1H, NH), 8.38 (s, 1H, NH), 7.17-7.19 (m, 2H, Ar-H), 7.75-7.82 (m, 2H, Ar-H), 5.78 (s, 1H, CH), 4.25 (q, 2H, CH_2), 2.84 (s, 3H, CH_3), 1.18 (t, 3H, CH_3).

4.A.6.4 Ethyl 1,2,3,4-tetrahydro-6-methyl-4-(4-nitrophenyl)-2-oxopyrimidine-5-carboxylate (4d): pale yellow solid, yield= 97 %, melting point found ($^{\circ}\text{C}$) = 208-210, IR (cm^{-1}) ν_{max} : 3455 cm^{-1} , 2966 cm^{-1} (N-H), 1659 cm^{-1} (C=O), ^1H NMR (400 MHz, DMSO d_6): δ_{ppm} = 9.29 (s, 1H, NH), 8.23 (d, 2H, Ar-H), 7.58 (d, 2H, Ar-H), 6.96 (s, 1H, Ar-H), 6.17(s, 1H, NH), 5.78 (d, 1H, CH), 3.38 (q, 2H, CH_2), 2.50 (s, 3H, CH_3), 1.08 (t, 3H, CH_3).

4.A.6.5 Ethyl 4-(3-bromophenyl)-1,2,3,4-tetrahydro-6-methyl-2-oxopyrimidine-5-carboxylate (4e): White Crystals, yield= 96 %, melting point found ($^{\circ}\text{C}$) = 189-191, IR (cm^{-1}) ν_{max} : 3448, 3240, 3112 (NH), 1672, 1621 (C=O), ^1H NMR (400 MHz, DMSO d_6): δ_{ppm} = 9.98 (s, 1H, NH), 7.95 (s, 1H, NH), 7.30-7.73 (m, 4H, Ar-H), 5.43 (d, 1H, CH), 4.24 (q, 2H, CH_2), 2.27 (s, 3H, CH_3), 1.23 (t, 3H, CH_3).

4.A.6.6 Ethyl 4-(2-chlorophenyl)-1,2,3,4-tetrahydro-6-methyl-2-oxopyrimidine-5-carboxylate (4f): White solid, yield= 97 %, melting point found ($^{\circ}\text{C}$) = 221-225, IR (cm^{-1}) ν_{max} : 3354 cm^{-1} , 3235, 3111 (N-H), 1662, 1640 cm^{-1} (C=O), ^1H NMR (400 MHz, DMSO d_6): δ_{ppm} = 9.32 (s, 1H, NH), 7.70(s, 1H, NH), 7.21-7.40(m, 4H, Ar-H), 5.59 (s, 1H, C-H), 4.11 (q, 2H, CH_2), 2.28 (s, 3H, CH_3), 1.08(t, 3H, CH_3).

4.A.6.7 Ethyl 4-(4-fluorophenyl)-1,2,3,4-tetrahydro-6-methyl-2-oxopyrimidine-5-carboxylate (4g): White Crystals, yield= 97 %, melting point found ($^{\circ}\text{C}$) = 208-212, IR (cm^{-1}) ν_{max} : 3326, 3200 (N-H), 1695, 1625 (C=O), ^1H NMR (400 MHz, DMSO- d_6): δ_{ppm} = 9.32(s, 1H, NH), 7.62(s, 1H, NH), 7.21-7.42(m, 4H, Ar-H), 5.22 (s, 1H, C-H), 3.85 (q, 2H, CH_2 of ethyl), 2.24 (s, 3H, CH_3), 1.12(t, 3H, CH_3).

4.A.6.8. Ethyl 1,2,3,4-tetrahydro-6-methyl-4-(2,4-dimethylphenyl)-2-oxopyrimidine-5-carboxylate (4h): White Crystals, yield= 93 %, melting point found ($^{\circ}\text{C}$) = 199-202, IR (cm^{-1}) ν_{max} : 3234, 3313, 3171, 2933 (N-H), 1700, 1648 (C=O), ^1H NMR (400 MHz, DMSO- d_6): δ_{ppm} = 9.24 (s, 1H, NH), 7.58 (s, 1H, NH), 6.68-6.78(m, 3H, Ar-H), 5.18 (s, 1H, C-H), 4.08(q, 2H, CH_2), 2.38(s, 3H, CH_3), 1.05(t, 3H, CH_3).

4.A.6.9 Ethyl 1,2,3,4-tetrahydro-4-(2,4-dihydroxyphenyl)-6-methyl-2-oxopyrimidine-5-carboxylate (4i): Pale brown Crystals, yield= 92 %, IR (cm^{-1}) ν_{max} : 3449, 3234 (N-H), 1664, 1626 (C=O), ^1H NMR (400 MHz, DMSO- d_6): δ_{ppm} = 12.97(s, 1H, OH), 11.79(s, 1H, OH), 10.18(s, 1H, NH), 8.51(s, 1H, NH), 6.79-7.18(m, 3H, Ar-H), 5.42 (d, 1H, C-H), 4.02(q, 2H, CH_2), 2.49 (s, 3H, CH_3), 1.25(t, 3H, CH_3).

4. A.6.10 Ethyl 1,2,3,4-tetrahydro-4-(2-hydroxyphenyl)-6-methyl-2-oxopyrimidine-5-carboxylate (4j): White solid, yield= 93 %, melting point found ($^{\circ}\text{C}$) = 203-206, IR (KBr, cm^{-1}) ν_{max} : 3348 (O-H), 3244, 3082 (N-H), 1686, 1638 (C=O), ^1H NMR (400 MHz, DMSO- d_6): δ_{ppm} = 13.34(s, 1H, OH), 8.94(s, 1H, NH), 8.93(s, 1H, NH), 6.84-7.38 (m, 3H, Ar-H), 6.82 (s, 1H, C-H), 3.38 (q, 2H, CH_2), 2.55(s, 3H, CH_3), 1.913(t, 3H, CH_3).

4.A.6.11 Ethyl 4-(5-chloro-2-hydroxyphenyl)-1,2,3,4-tetrahydro-6-methyl-2-oxopyrimidine-5-carboxylate (4k): Dirty white solid, melting point found ($^{\circ}\text{C}$) = 208-211, IR (KBr, cm^{-1}) ν_{max} : 3443 (OH), 3298, 2955 (NH), 1666, 1625 (C=O), ^1H NMR (400 MHz, DMSO- d_6): δ_{ppm} = 9.36 (s, 1H, OH), 7.54(s, 1H, NH), 7.52(s, 1H, NH), 7.30-7.43(m, 3H, Ar-H), 5.48 (d, 1H, C-H), 3.45 (q, 2H, CH_2), 2.45(s, 3H, CH_3), 1.29(t, 3H, CH_3).

4. A.6.12 Ethyl 1,2,3,4-tetrahydro-4-(2-hydroxy-5-nitrophenyl)-6-methyl-2-oxopyrimidine-5-carboxylate (5l): yellow solid, IR (KBr, cm^{-1}) ν_{max} : 3442 (OH), 3125, 2954, 2924 (NH), 1731, 1681 (C=O), ^1H NMR (400 MHz, DMSO- d_6): δ_{ppm} = 9.91(s, 1H, OH), 8.53(s, 1H, NH), 8.40(s, 1H, NH), 7.48-7.82(m, 2H, Ar-H), 6.91-6.89 (d, 1H, Ar-H), 5.43(d, 1H, CH), 3.40(m, 2H, CH_2), 2.25(s, 3H, CH_3), 2.51(t, 3H, CH_3).

4. A.6.13 Ethyl 1,2,3,4-tetrahydro-4-(4-hydroxy-3-methoxyphenyl)-6-methyl-2-oxopyrimidine-5-carboxylate (4m): yellow solid, IR (KBr, cm^{-1}) ν_{max} : 3425 (OH), 3348 3125, 2974, 2924 (NH), 1731, 1681 (C=O), ^1H NMR (400 MHz, DMSO- d_6): δ = 9.12(s, 1H, OH), 8.51(s, 1H, NH), 7.63(s, 1H, NH), 6.51-6.79(m,

3H, Ar-H), 5.42(d, 1H, CH), 4.00 (s, 3H, OCH₃), 3.72(m, 2H, CH₂), 2.47(s, 3H, CH₃), 1.16(t, 3H, CH₃).

4.A.6.14 Ethyl 1,2,3,4-tetrahydro-4-(3-hydroxyphenyl)-6-methyl-2-oxopyrimidine-5-carboxylate (4n): Dirty white powder, yield= 88 %, melting point found (°C) = 258-261. IR (KBr, cm⁻¹) v_{max}:3443 (O-H), 3244, 3110, 2950(N-H), 1647, 1578(C=O), ¹HNMR (400 MHz, DMSO-d₆): δppm= 9.97(s, 1H, OH), 9.35(s, 1H, NH),7.66(s, 1H, NH), 6.50-6.74(m, 3H, Ar-H), 5.62(s, 1H, -C-H), 3.37 (q, 2H, CH₂), 2.22(s, 3H, CH₃), 1.10 (t, 3H, CH₃).

4.A.6.15 Ethyl 1,2,3,4-tetrahydro-4-(3,4,5-trimethoxyphenyl)-6-methyl-2-oxopyrimidine-5-carboxylate (4o): White solid , yield= 88 %, melting point found (°C) =202-206, IR (KBr, cm⁻¹) v_{max}: 3443 (O-H), 3364, 3302, 2971(N-H), 1660, 1595(C=O), ¹HNMR (400 MHz, DMSO-d₆): δppm= 9.80(s, 1H, OH), 9.20(s, 1H, NH),7.25(s, 1H, NH), 6.87(s, 1H, Ar-H), 6.64 (s, 1H, Ar-H), 5.40(s, 1H, C-H), 3.85(q, 2H, CH₂), 3.71(s, 3H, O-CH₃),3.67(s, 3H, O-CH₃), 3.62(s, 3H, O-CH₃), 3.37(s, 3H, CH₃), 1.27 (t, 3H, CH₃).

4.A.6.16 Ethyl 1,2,3,4-tetrahydro-4-(4-hydroxy-3,5-dimethoxyphenyl)-6-methyl-2-oxopyrimidine-5-carboxylate (4p): Dirty white solid, yield=88 %, IR (KBr, cm⁻¹) v_{max}: 3433 (O-H), 3302, 2970, 2926(N-H), 1665, 1627 (C=O), ¹HNMR (400 MHz, DMSO-d₆): δppm= 11.40 (s, 1H, OH), 9.77(s, 1H, NH), 8.31(s, 1H, NH), 7.20(s, 1H, Ar-H), 6.92 (s, 1H, Ar-H), 5.39(s, 1H, C-H), 3.88 (s, 6H, OCH₃), 3.31(q, 2H, CH₂), 2.49(s, 3H, CH₃), 1.21 (t, 3H, CH₃).

4.A.6.17 Ethyl 1,2,3,4-tetrahydro-4-(1H-indol-3-yl)-6-methyl-2-oxopyrimidine-5-carboxylate (4q): brown solid, IR (KBr, cm⁻¹) v_{max}: 3445, 2932 (N-H), 1662, 1632 (C=O), ¹HNMR (400 MHz, DMSO-d₆): δppm= 12.14 (s, 1H, NH indole), 9.92(s, 1H, NH), 8.32(s, 1H, NH), 8.27 (m, 1H Ar-H indole), 7.18-7.51(m, 4H, Ar-H), 5.41(s, 1H, C-H), 3.33(q, 2H, CH₂), 2.49(s, 3H, CH₃), 1.81 (t, 3H, CH₃).

4.A.7 Supporting spectra:

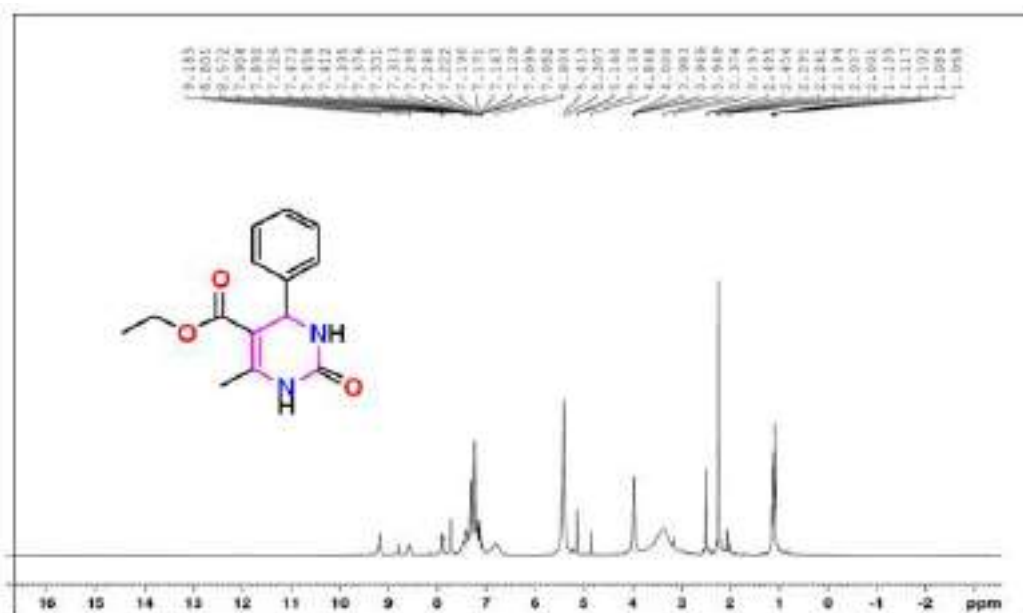


Fig. 4.A.7.1. ^1H NMR spectra of Ethyl 1,2,3,4-tetrahydro-6-methyl-2-oxo-4-phenylpyrimidine-5-carboxylate (4a)

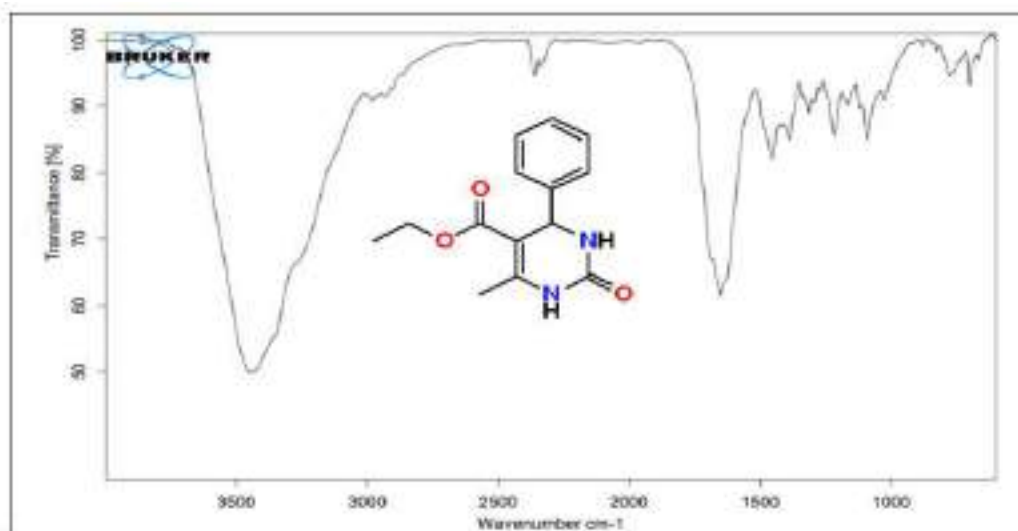


Fig. 4.A.7.2. FT-IR spectra of Ethyl 1,2,3,4-tetrahydro-6-methyl-2-oxo-4-phenylpyrimidine-5-carboxylate (4a)

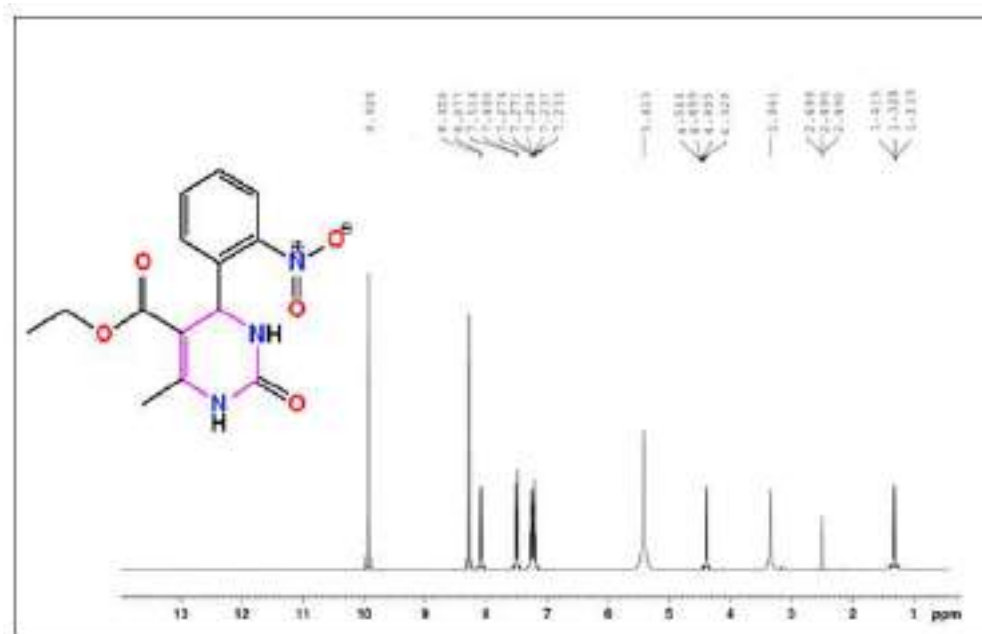


Fig. 4.A.7.3. ¹H NMR spectra of Ethyl 1,2,3,4-tetrahydro-6-methyl-4-(2-nitrophenyl)-2-oxopyrimidine-5-carboxylate (4b)

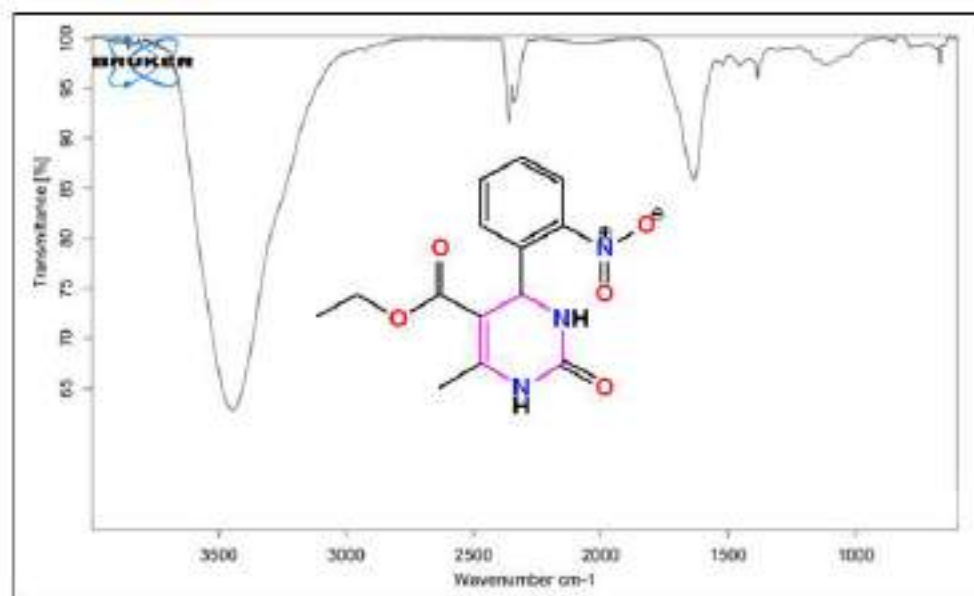


Fig. 4.A.7.4. FT-IR spectra of Ethyl 1,2,3,4-tetrahydro-6-methyl-4-(2-nitrophenyl)-2-oxopyrimidine-5-carboxylate (4b)

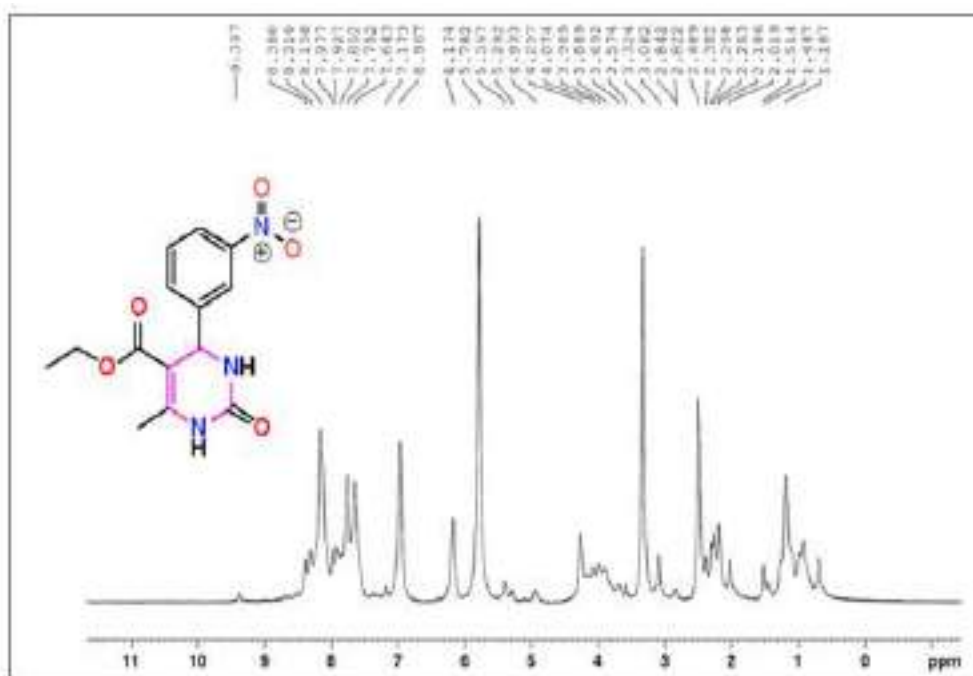


Fig. 4.A.7.5. ^1H NMR spectra of Ethyl 1,2,3,4-tetrahydro-6-methyl-4-(3-nitrophenyl)-2-oxopyrimidine-5-carboxylate (4c).

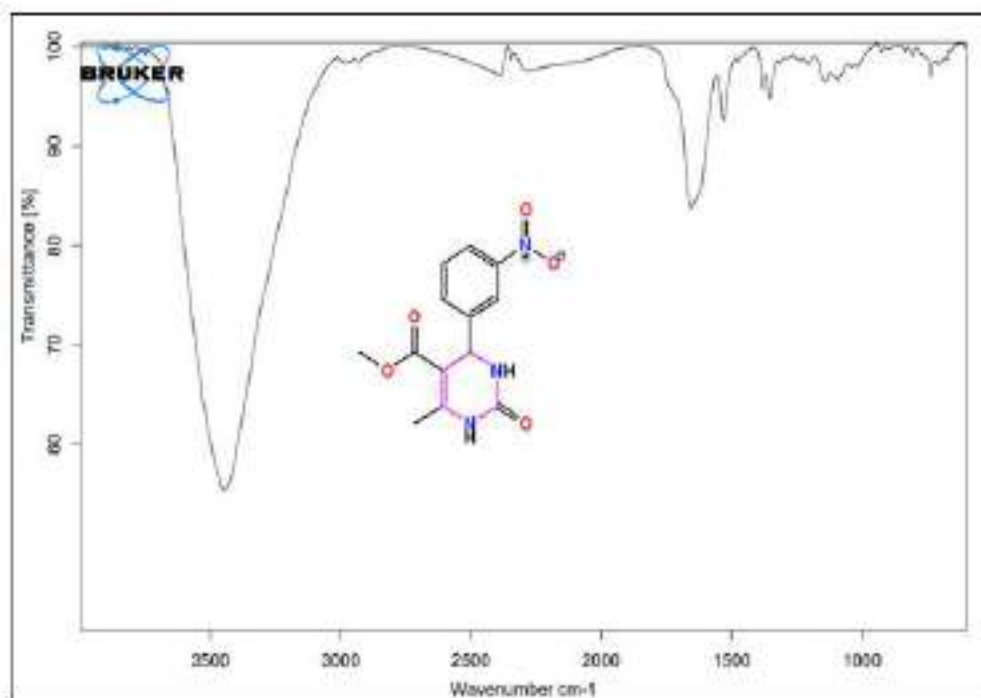


Fig. 4.A.7.6. FT-IR spectra of Ethyl 1,2,3,4-tetrahydro-6-methyl-4-(3-nitrophenyl)-2-oxopyrimidine-5-carboxylate (4c)

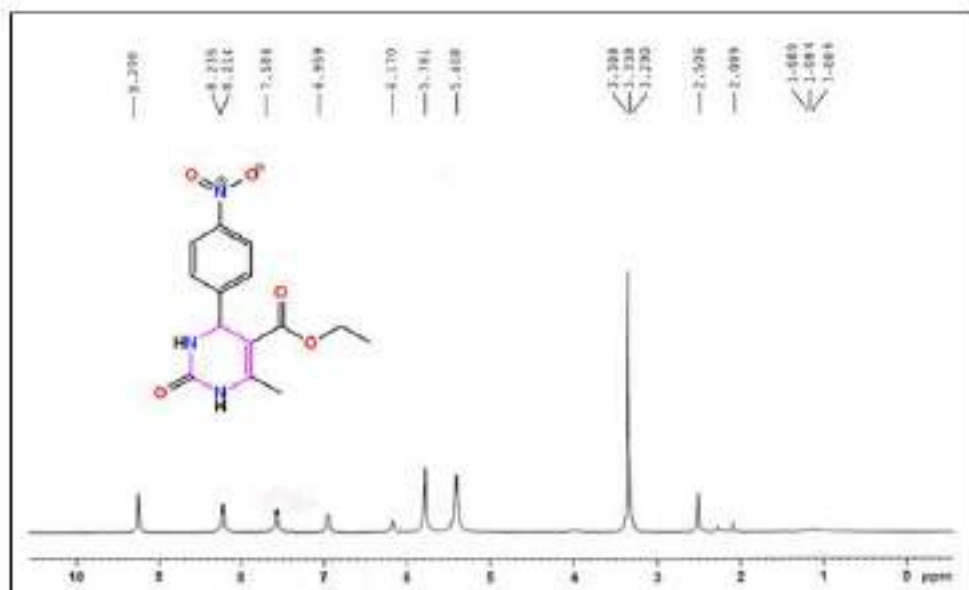


Fig. 4.A.7.7. ¹H NMR spectra of Ethyl 1,2,3,4-tetrahydro-6-methyl-4-(4-nitrophenyl)-2-oxopyrimidine-5-carboxylate (4d).

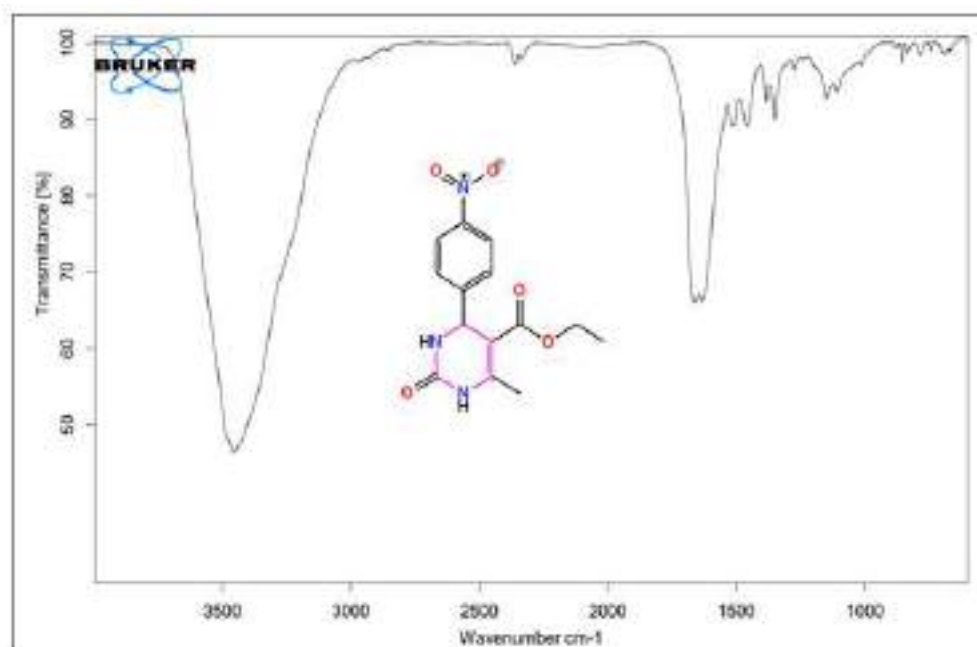


Fig. 4.A.7.8. FT-IR spectra of Ethyl 1,2,3,4-tetrahydro-6-methyl-4-(4-nitrophenyl)-2-oxopyrimidine-5-carboxylate (4d)

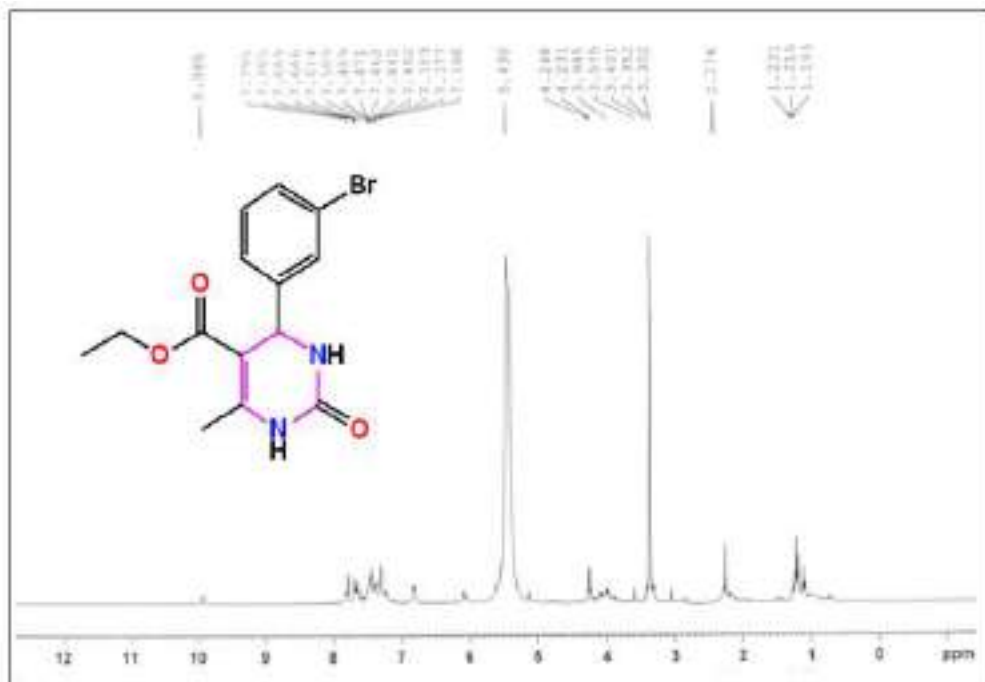


Fig.4. A.7.9. ^1H NMR spectra of Ethyl 4-(3-bromophenyl)-1,2,3,4-tetrahydro-6-methyl-2-oxypyrimidine-5-carboxylate (4e).

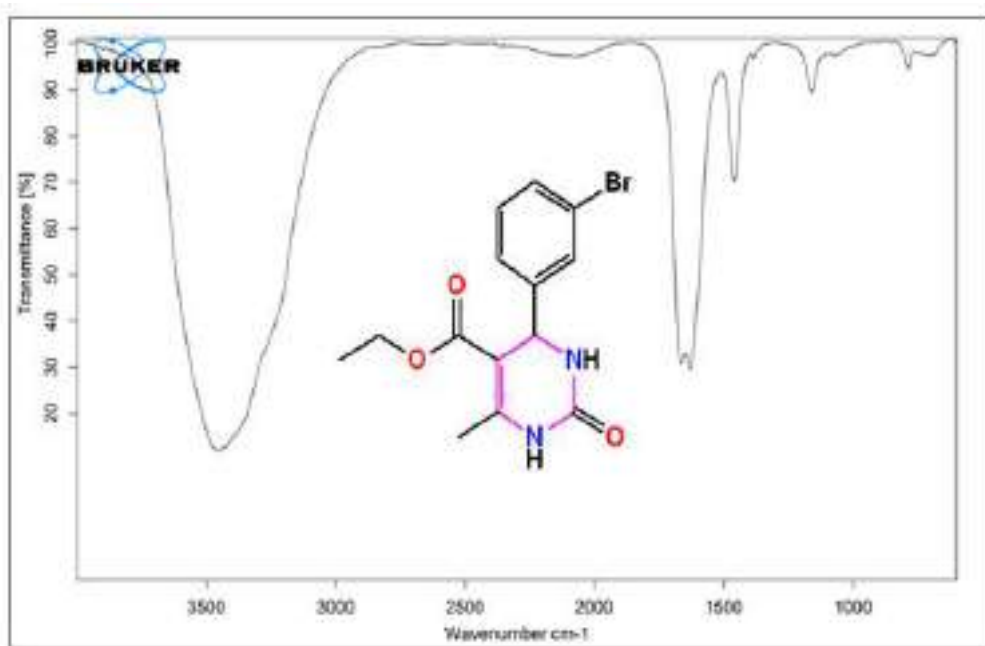


Fig. 4.A.7.10. FT-IR spectra of Ethyl 4-(3-bromophenyl)-1,2,3,4-tetrahydro-6-methyl-2-oxypyrimidine-5-carboxylate (4e).

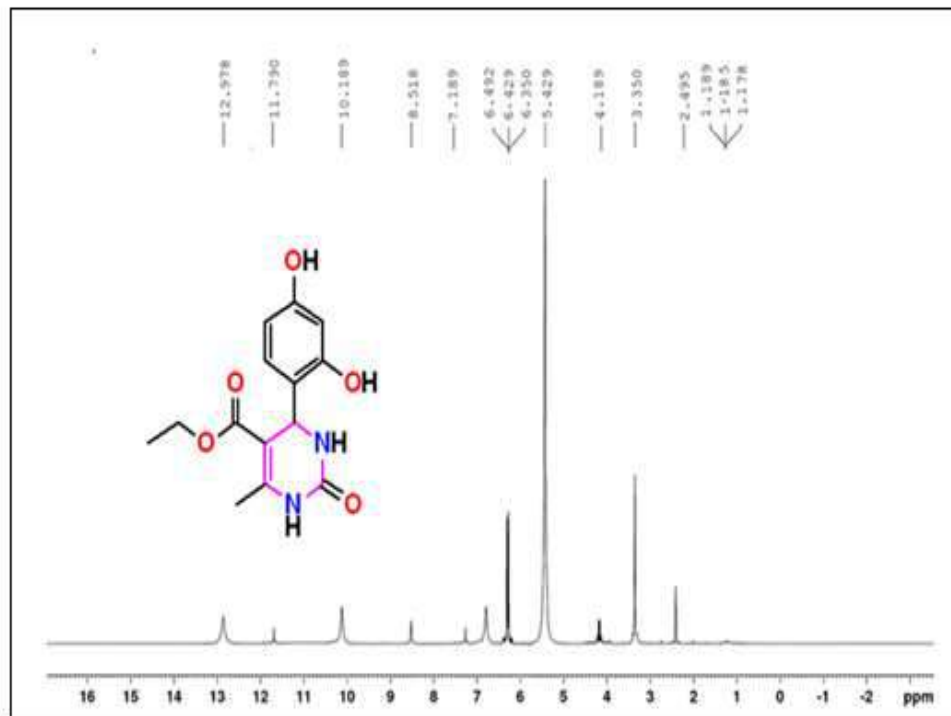


Fig. 4.A.7.11. ^1H NMR spectra of Ethyl 1,2,3,4-tetrahydro-4-(2,4-dihydroxyphenyl)-6-methyl-2-oxopyrimidine-5-carboxylate (4i).

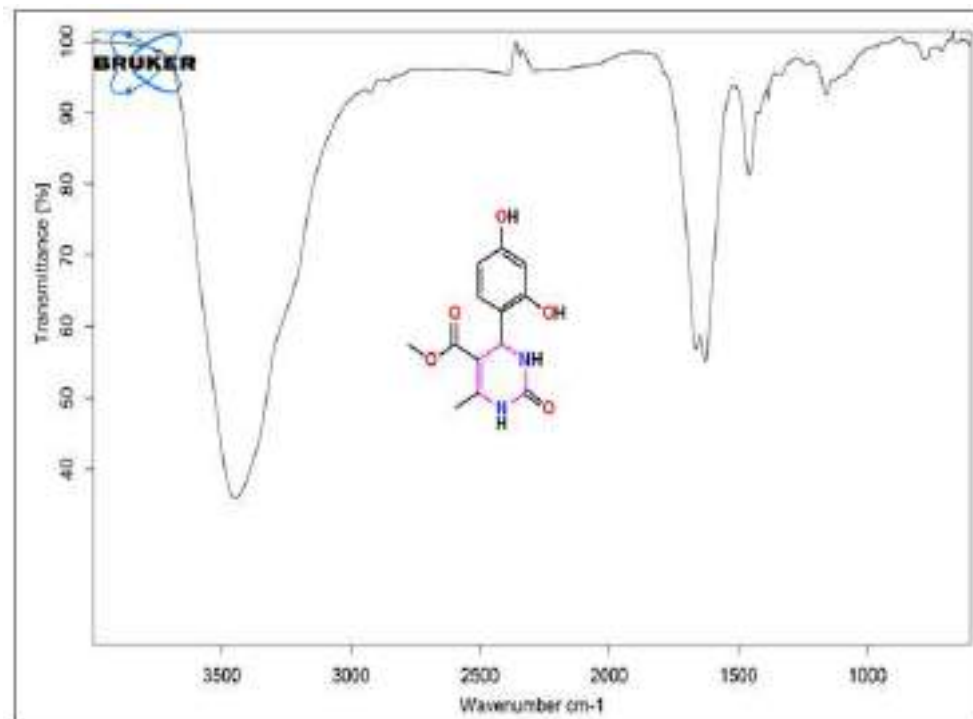


Fig. 4.A.7.12. FT-IR spectra of Ethyl 1,2,3,4-tetrahydro-4-(2,4-dihydroxyphenyl)-6-methyl-2-oxopyrimidine-5-carboxylate (4i).

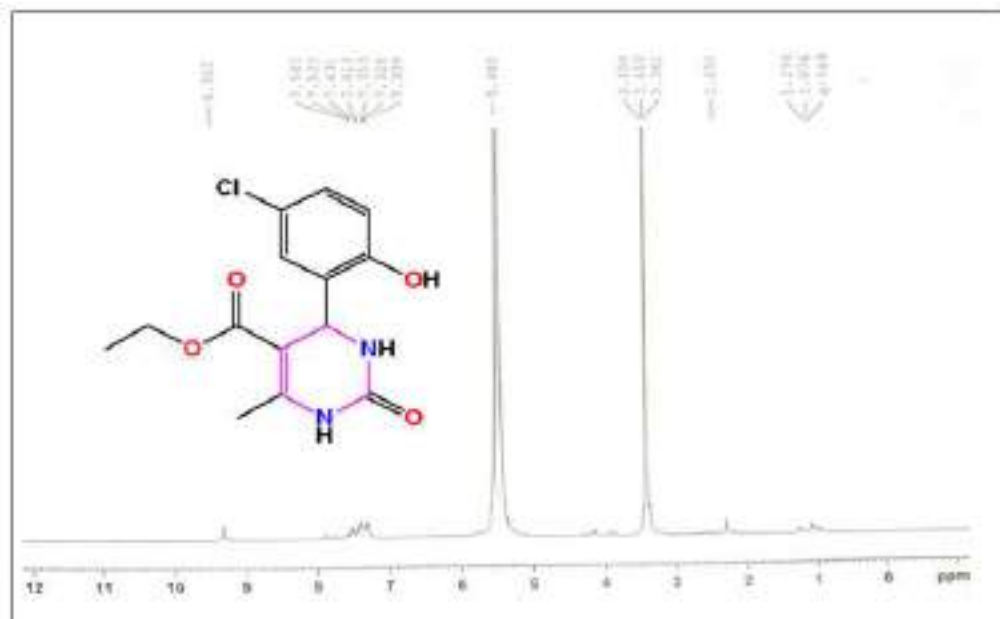


Fig. 4.A.7.13. ¹H NMR spectra of Ethyl 4-(5-chloro-2-hydroxyphenyl)-1,2,3,4-tetrahydro-6-methyl-2-oxypyrimidine-5-carboxylate (4k).

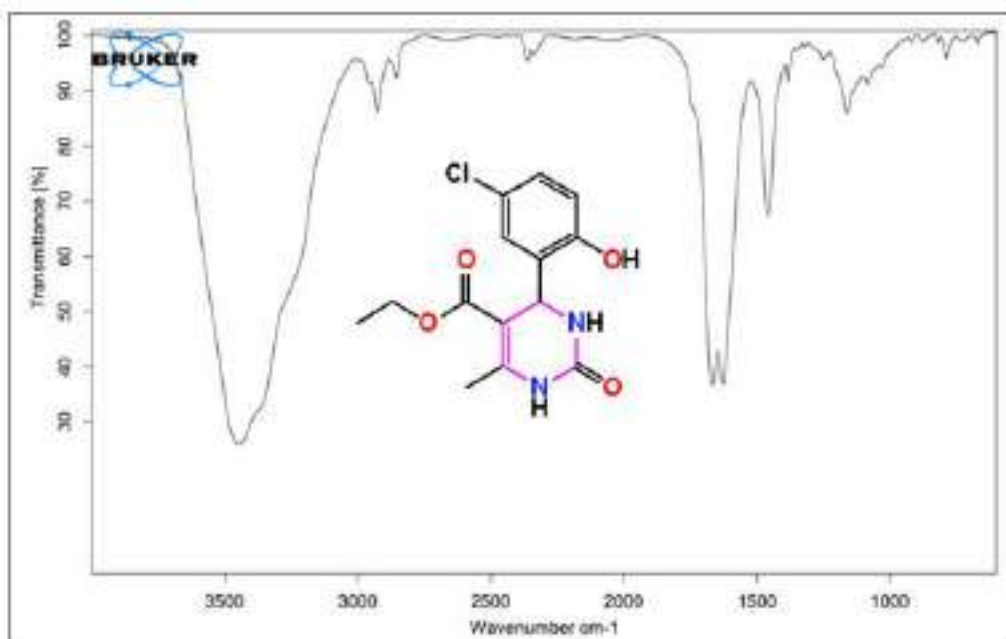


Fig. 4.A.7.14. FT-IR spectra of Ethyl 4-(5-chloro-2-hydroxyphenyl)-1,2,3,4-tetrahydro-6-methyl-2-oxypyrimidine-5-carboxylate (4k).

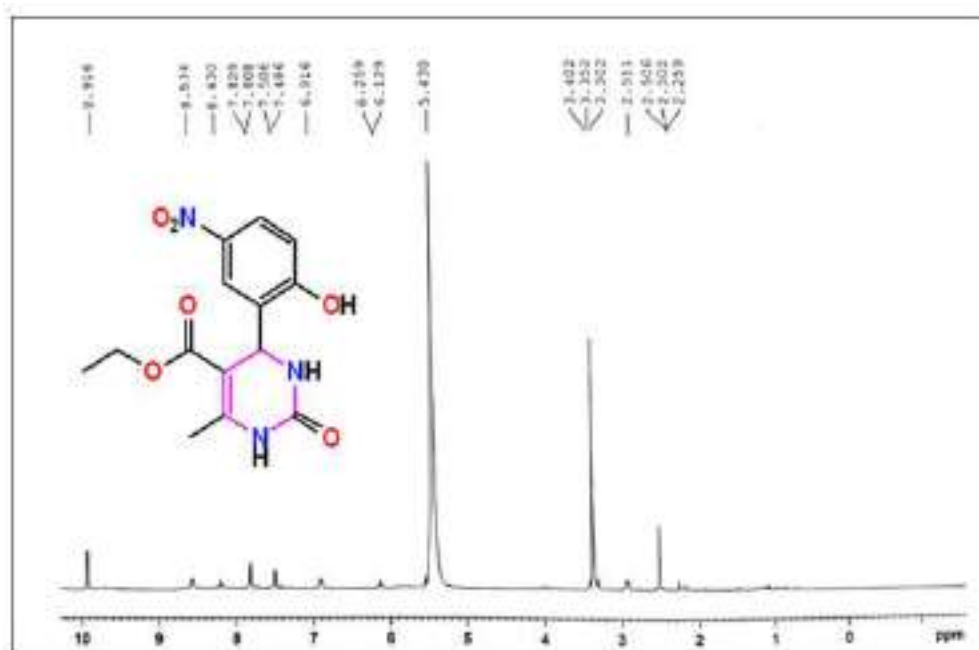


Fig. 4.A.7.15. ¹H NMR spectra of Ethyl 1,2,3,4-tetrahydro-4-(2-hydroxy-5-nitrophenyl)-6-methyl-2-oxopyrimidine-5-carboxylate (4l).

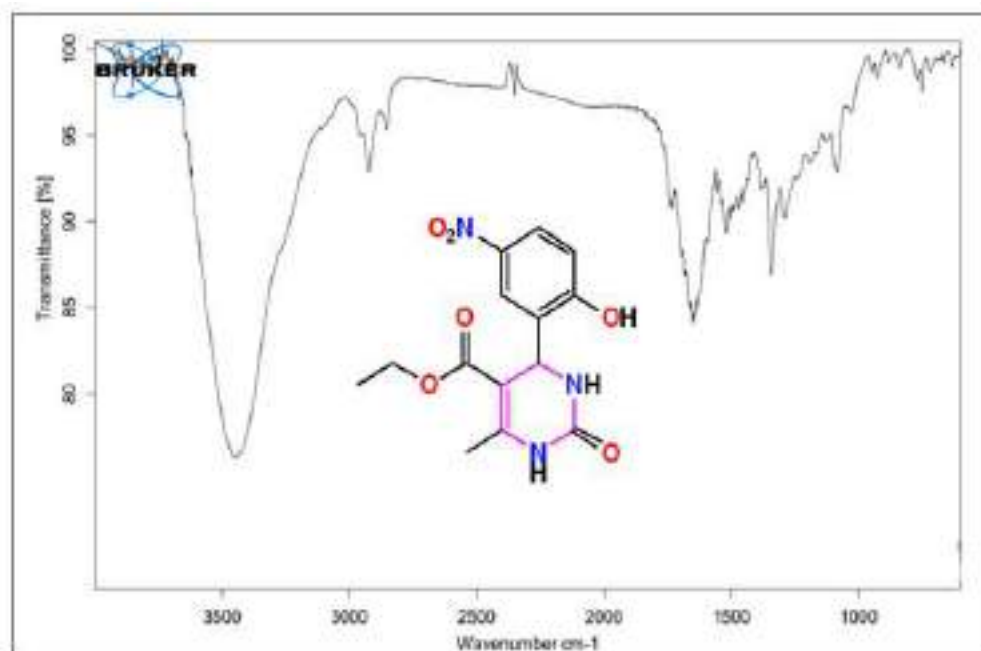


Fig. 4.A.7.16. FT-IR spectra of Ethyl 1,2,3,4-tetrahydro-4-(2-hydroxy-5-nitrophenyl)-6-methyl-2-oxopyrimidine-5-carboxylate (4l).

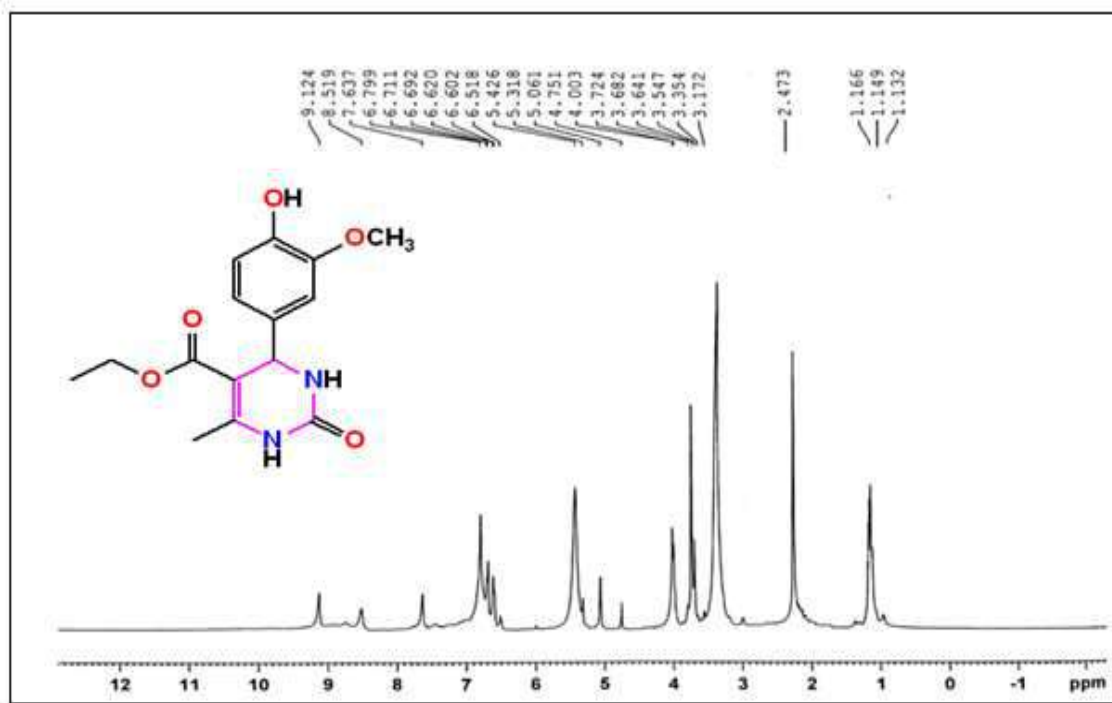


Fig. 4.A.7.17. ^1H NMR spectra of Ethyl 1,2,3,4-tetrahydro-4-(4-hydroxy-3-methoxyphenyl)-6-methyl-2-oxopyrimidine-5-carboxylate (4m).

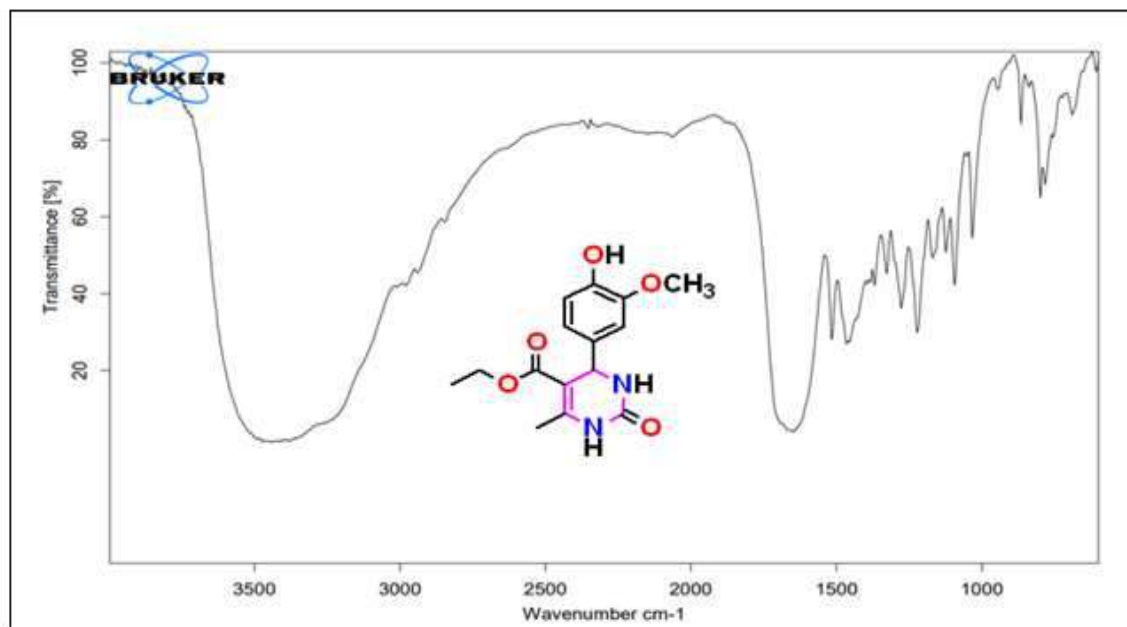


Fig. 4.A.7.18. FT-IR spectra of Ethyl 1,2,3,4-tetrahydro-4-(4-hydroxy-3-methoxyphenyl)-6-methyl-2-oxopyrimidine-5-carboxylate (4m).

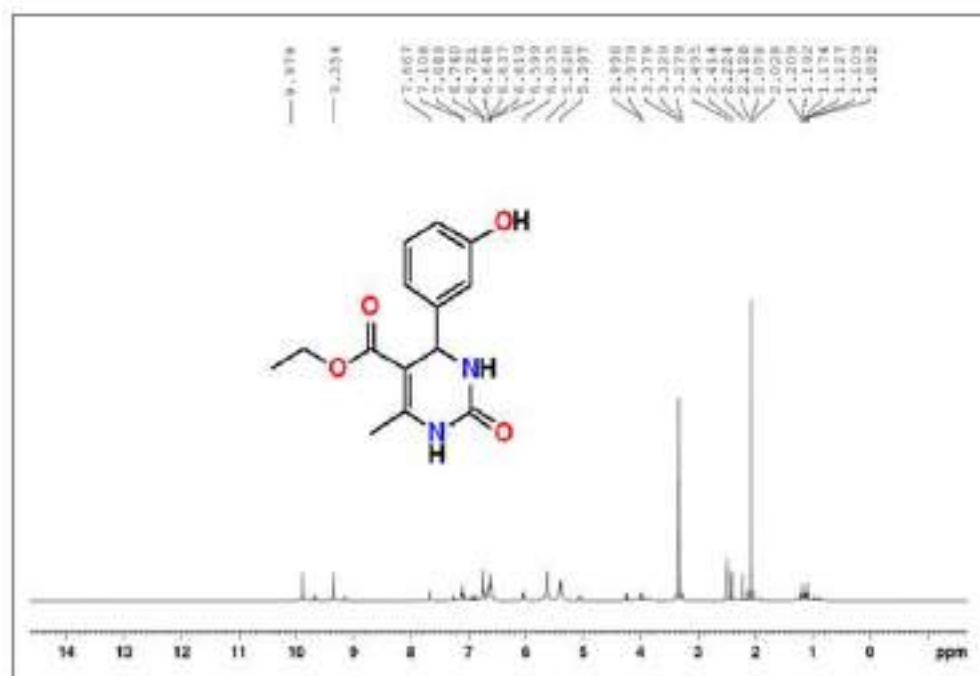


Fig. 4.A.7.19. ¹H NMR spectra of Ethyl 1,2,3,4-tetrahydro-4-(3-hydroxyphenyl)-6-methyl-2-oxopyrimidine-5-carboxylate (4n)

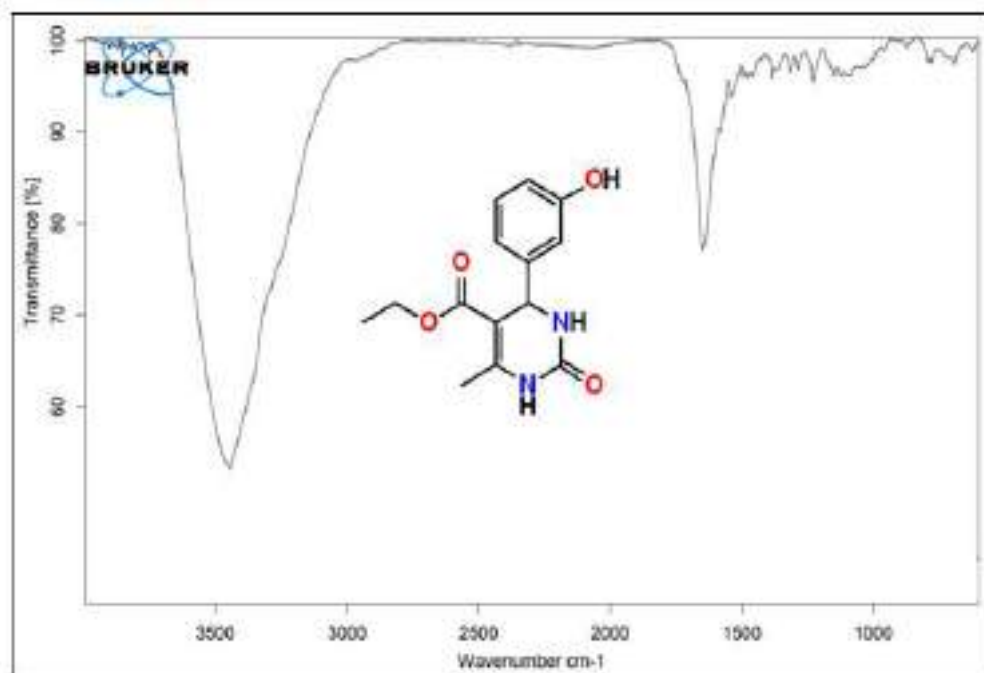


Fig. 4.A.7.20. FT-IR spectra of Ethyl 1,2,3,4-tetrahydro-4-(3-hydroxyphenyl)-6-methyl-2-oxopyrimidine-5-carboxylate (4n)

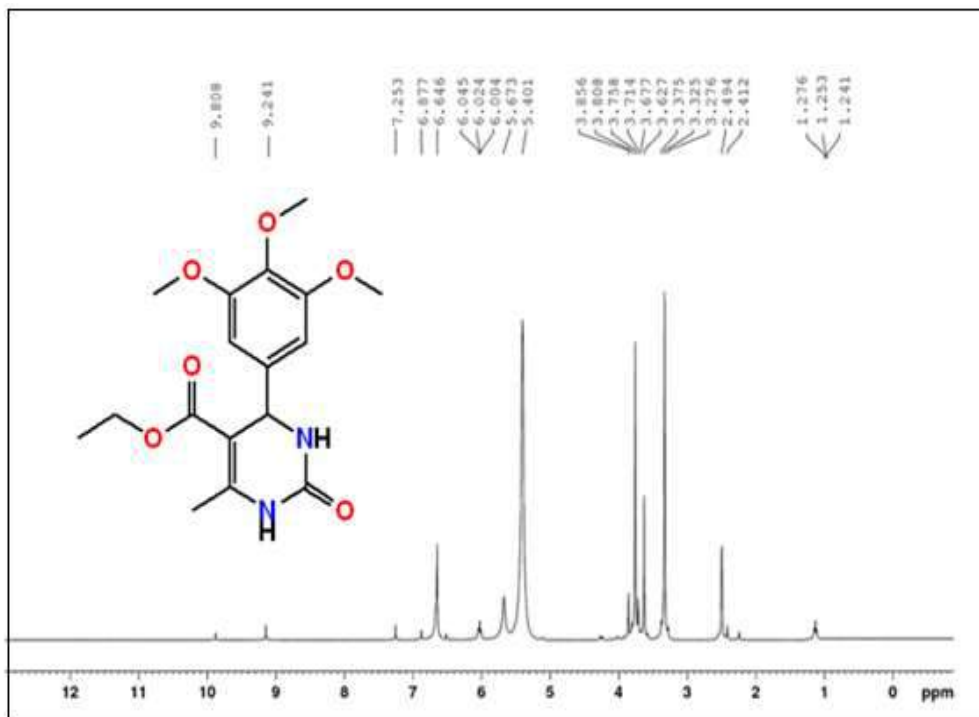


Fig. 4.A.7.21. ¹H NMR spectra of Ethyl 1,2,3,4-tetrahydro-4-(3,4,5-trimethoxyphenyl)-6-methyl-2-oxopyrimidine-5-carboxylate (4o).

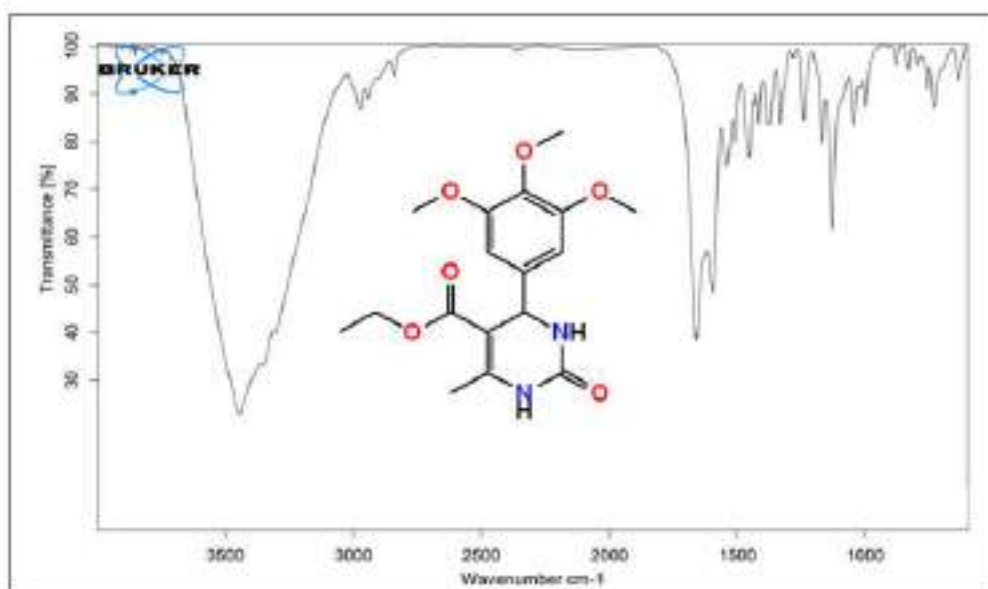


Fig. 4.A.7.22. FT-IR spectra of Ethyl 1,2,3,4-tetrahydro-4-(3,4,5-trimethoxyphenyl)-6-methyl-2-oxopyrimidine-5-carboxylate.

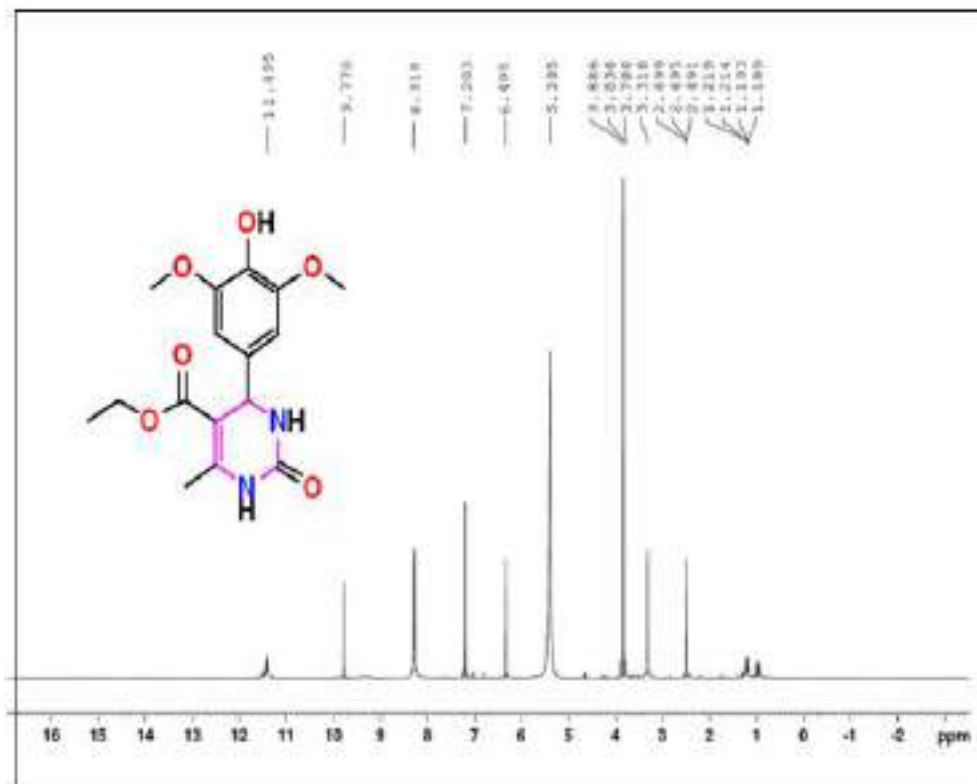


Fig. 4.A.7.23. ^1H NMR spectra of Ethyl 1,2,3,4-tetrahydro-4-(4-hydroxy-3,5-dimethoxyphenyl)-6-methyl-2-oxopyrimidine-5-carboxylate (4p)

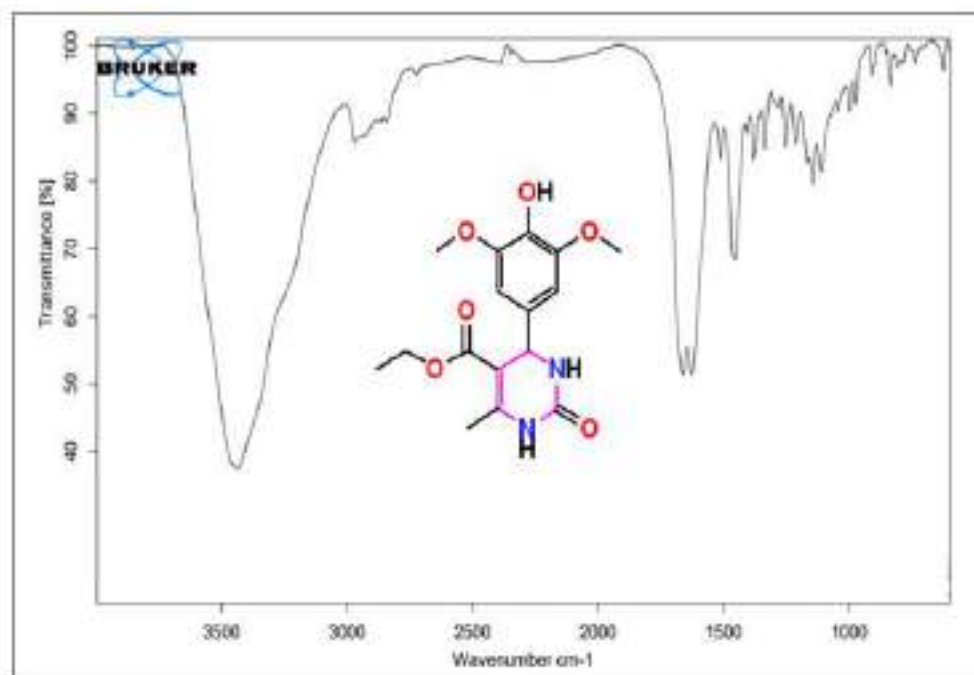


Fig. 4.A.7.24. FT-IR spectra of Ethyl 1,2,3,4-tetrahydro-4-(4-hydroxy-3,5-dimethoxyphenyl)-6-methyl-2-oxopyrimidine-5-carboxylate (4p)

4.A.8 References

- (1) S. Zangade, P. Patil., *Current Organic Chemistry*, **2019**, 23 (21), 2295–2318.
- (2) T. T. Nguyen, P. H. Tran., *RSC Advances*, **2020**, 10 (16), 9663–9671.
- (3) L. Biesen, T. J. J. Müller., *Advanced Synthesis & Catalysis*, **2021**, 363 (4), 980–1006.
- (4) B. M. Sahoo, B. V. V. R. Kumar, J. Panda, S. C. Dinda., *Journal of Nanoparticles*, **2013**, 2013 (Article ID 780786), 1–6.
- (5) P. Costanzo, M. Nardi, M. Oliverio., *European Journal of Organic Chemistry*, **2020**, 2020 (26), 3954–3964.
- (6) B. Mohammadi, F. K. Behbahani., *Molecular Diversity*, **2018**, 22 (2), 405–446.
- (7) R. Kaur, S. Chaudhary, K. Kumar, M. K. Gupta, R. K. Rawal., *European Journal of Medicinal Chemistry*, **2017**, 132, 108–134.
- (8) J. Lloyd, H. J. Finlay, K. Atwal, A. Kover, J. Prol, L. Yan, R. Bhandaru, W. Vaccaro, T. Huynh, C. S. Huang, M. L. Conder, T. Jenkins-West, H. Sun, D. Li, P. Levesque., *Bioorganic & Medicinal Chemistry Letters*, **2009**, 19 (18), 5469–5473.
- (9) J. Lloyd, H. J. Finlay, W. Vacarro, T. Hyunh, A. Kover, R. Bhandaru, L. Yan, K. Atwal, M. L. Conder, T. Jenkins-West, H. Shi, C. Huang, D. Li, H. Sun, P. Levesque., *Bioorganic & Medicinal Chemistry Letters*, **2010**, 20 (4), 1436–1439.
- (10) E. W. Hurst, R. Hull., *Journal of Medicinal Chemistry*, **1961**, 3 (2), 215–229.
- (11) C. O. Kappe., *European Journal of Medicinal Chemistry*, **2000**, 35 (12), 1043–1052.
- (12) L. M. Ramos, B. C. Guido, C. C. Nobrega, J. R. Corrêa, R. G. Silva, H. C. B. de Oliveira, A. F. Gomes, F. C. Gozzo, B. A. D. Neto., *Chemistry – A European Journal*, **2013**, 19 (13), 4156–4168.
- (13) R. Sharma, S. S. Jadav, S. Yasmin, S. Bhatia, H. Khalilullah, M. J. Ahsan., *Medicinal Chemistry Research*, **2015**, 24 (2), 636–644.
- (14) C. A. Bewley, S. Ray, F. Cohen, S. K. Collins, L. E. Overman., *Journal of Natural Products*, **2004**, 67 (8), 1319–1324.
- (15) S. Tcherniuk, R. van Lis, F. Kozielski, D. A. Skoufias., *Biochemical Pharmacology*, **2010**, 79 (6), 864–872.
- (16) G. Fitzharris., *Curr Biol*, **2012**, 22 (5), 437–444.
- (17) B. N. Acharya, G. B. D. Rao, D. Kumar, P. Kumar, M. P. Kaushik., *Medicinal Chemistry Research*, **2015**, 24 (4), 1763–1775.

- (18) P. Lacotte, D. A. Buisson, Y. Ambroise., *European Journal of Medicinal Chemistry*, **2013**, *62*, 722–727.
- (19) N. Singh, J. Kaur, P. Kumar, S. Gupta, N. Singh, A. Ghosal, A. Dutta, A. Kumar, R. Tripathi, M. I. Siddiqi, C. Mandal, A. Dube., *Parasitology Research*, **2009**, *105* (5), 1317–1325.
- (20) K. L. Dhumaskar, S. N. Meena, S. C. Ghadi, S. G. Tilve., *Bioorganic & Medicinal Chemistry Letters*, **2014**, *24* (13), 2897–2899.
- (21) A. Khan, J. Hashim, N. Arshad, I. Khan, N. Siddiqui, A. Wadood, M. Ali, F. Arshad, K. M. Khan, M. I. Choudhary., *Bioorganic Chemistry*, **2016**, *64*, 85–96.
- (22) F. Celik, M. Arslan, M. O. Kaya, E. Yavuz, N. Gencer, O. Arslan., *Artificial Cells, Nanomedicine and Biotechnology*, **2014**, *42* (1), 58–62.
- (23) A. O. Bryzgalov, M. P. Dolgikh, I. v. Sorokina, T. G. Tolstikova, V. F. Sedova, O. P. Shkurko., *Bioorganic & Medicinal Chemistry Letters*, **2006**, *16* (5), 1418–1420.
- (24) F. Cohen, L. E. Overman, S. K. Ly Sakata., *Organic Letters*, **1999**, *1* (13), 2169–2172.
- (25) S. Mondal, M. A. Mondal., *Journal of Heterocyclic Chemistry*, **2020**, *57* (12), 4175–4180.
- (26) M. Khashaei, L. Kafi-Ahmadi, S. Khademinia, A. Poursattar Marjani, E. Nozad., *Scientific Reports*, **2022**, *12* (1), 1–15.
- (27) Z. Karimi-Jaberi, M. S. Moaddeli., *ISRN Organic Chemistry*, **2012**, *2012* (Article ID 474626).
- (28) S. J. Kim, S. R. McAlpine., *Molecules*, **2013**, *18* (1), 1111–1121.
- (29) P. Biginelli., *Berichte der deutschen chemischen Gesellschaft*, **1891**, *24* (2), 2962–2967.
- (30) S. S. Panda, P. Khanna, L. Khanna., *Current Organic Chemistry*, **2012**, *16* (4), 507–520.
- (31) E. Kolvari, N. Koukabi, O. Armandpour., *Tetrahedron*, **2014**, *70* (6), 1383–1386.
- (32) B. K. Banik, A. T. Reddy, A. Datta, C. Mukhopadhyay., *Tetrahedron Letters*, **2007**, *48* (41), 7392–7394.
- (33) V. Polshettiwar, R. S. Varma., *Tetrahedron Letters*, **2007**, *48* (41), 7343–7346.
- (34) K. K. Pasunooti, H. Chai, C. N. Jensen, B. K. Gorityala, S. Wang, X. W. Liu., *Tetrahedron Letters*, **2011**, *52* (1), 80–84.

- (35) F. Dong, L. Jun, Z. Xinli, Y. Zhiwen, L. Zuliang., *Journal of Molecular Catalysis A: Chemical*, **2007**, 274 (1), 208–211.
- (36) A. Kuraitheerthakumaran, S. Pazhamalai, M. Gopalakrishnan., *Arabian Journal of Chemistry*, **2016**, 9 (Suppl. 1), S461–S465.
- (37) X. Chen, Y. Peng., *Catalysis Letters*, **2008**, 122 (3–4), 310–313.
- (38) S. L. Jain, J. K. Joseph, B. Sain., *Catalysis Letters*, **2007**, 115 (1–2), 52–55.
- (39) C. Ramalingan, S. J. Park, I. S. Lee, Y. W. Kwak., *Tetrahedron*, **2010**, 66 (16), 2987–2994.
- (40) F. Tamaddon, Z. Razmi, A. A. Jafari., *Tetrahedron Letters*, **2010**, 51 (8), 1187–1189.
- (41) H. Valizadeh, A. Shockravi., *Heteroatom Chemistry*, **2009**, 20 (5), 284–288.
- (42) Y. Zhang, B. Wang, X. Zhang, J. Huang, C. Liu., *Molecules*, **2015**, 20 (3), 3811–3820.
- (43) S. P. Bahekar, P. B. Sarode, M. P. Wadekar, H. S. Chandak., *Journal of Saudi Chemical Society*, **2017**, 21 (4), 415–419.
- (44) A. Khorshidi, K. Tabatabaieian, H. Azizi, M. Aghaei-Hashjin, E. Abbaspour-Gilandeh., *RSC Advances*, **2017**, 7 (29), 17732–17740.
- (45) M. M. Khodaei, A. R. Khosropour, M. Beygzadeh., *Synthetic Communications*, **2004**, 34 (9), 1551–1557.
- (46) S. Asghari, M. Tajbakhsh, B. J. Kenari, S. Khaksar., *Chinese Chemical Letters*, **2011**, 22 (2), 127–130.
- (47) X. H. Chen, X. Y. Xu, H. Liu, L. F. Cun, L. Z. Gong., *J Am Chem Soc*, **2006**, 128 (46), 14802–14803.
- (48) J. Safaei Ghomi, R. Teymuri, A. Ziarati., *Monatshefte fur Chemie*, **2013**, 144 (12), 1865–1870.
- (49) M. Zeinali-Dastmalbaf, A. Davoodnia, M. M. Heravi, N. Tavakoli-Hoseini, A. Khojastehnezhad, H. A. Zamani., *Bull Korean Chem Soc*, **2011**, 32 (2), 656–658.
- (50) S. D. Salim, K. G. Akamanchi., *Catalysis Communications*, **2011**, 12 (12), 1153–1156.
- (51) S. Rostamnia, A. Morsali., *RSC Advances*, **2014**, 4 (21), 10514–10518.
- (52) S. Chancharunee, P. Pinhom, M. Pohmakotr, P. Perlmutter., *Synthetic Communications*, **2009**, 39 (5), 880–886.

- (53) N. Firoozeh, S. Rezazadeh, C. Izanloo., *J Mex Chem Soc*, **2017**, *61* (3), 241–249.
- (54) M. Nasr-Esfahani, M. Montazerozohori, M. Aghel-Mirrezaee, H. Kashi., *Journal of the Chilean Chemical Society*, **2014**, *59* (1), 2311–2314.

CHAPTER-IV

Section-B

DFT, Molecular Docking and Pharmacokinetic study of some selected 3, 4-dihydropyrimidin-2(1H)-one (DHPM) derivatives

4.B.1 Background of the present investigation

Dihydropyrimidin-2(1H)-ones are a class of organic compounds which are synthesized using Bigenelli reaction and have significant biological activity¹. Dihydropyrimidinones also called as Bigenelli compounds were first prepared by Pietro Bigenelli in the year 1893¹. These classes of compounds have shown promising biological activities like calcium channel anragonists²⁻³, anti-cancer⁴⁻⁵, anti-hypertensive⁶, anti-bacterial⁷, anti-inflammatory⁸, $\alpha_1\alpha$ adrenergic antagonists⁹ and HIV-gp-120-CD4 inhibitors¹⁰. Apart from biological activities, DHPMs are also used as essential building blocks for a variety of other heterocyclic compounds¹¹⁻¹⁷(Fig.4.B.1). Computational chemistry and theoretical calculations based on physicochemical and quantum mechanics involving organic molecules are gaining a lot interest these days as it helps in understanding the geometrical properties, reaction pathways and chemical mechanisms¹⁸⁻¹⁹. Also, these theoretical techniques provide information about the electronic properties of the reactants, intermediates and products which helps in inculcating new ideas for planning an organic synthesis²⁰⁻²¹. Recently, Density Functional Theory (DFT) is mostly used for exploring the geometry and electronic properties of organic molecules along with some important properties like dipole moments, optical properties, vibration frequencies and thermodynamic properties²²⁻²⁴. The information obtained from theoretical calculations can be compared with the experimental finding which helps to gain a deep insight into the various properties of the compounds under study. With the advancement in computational chemistry, Computer Aided Drug Design (CADD) is an emerging field of research²⁵ and it helps to predict the different types of interaction prevailing between the ligand and active site of the protein²⁶. Usually, the development of a new drug for a particular disease is a very long tedious and also a costly process²⁷ and therefore, CADD method is widely used for drug designing as it efficiently reduces the time and cost for drug discovery²⁸.

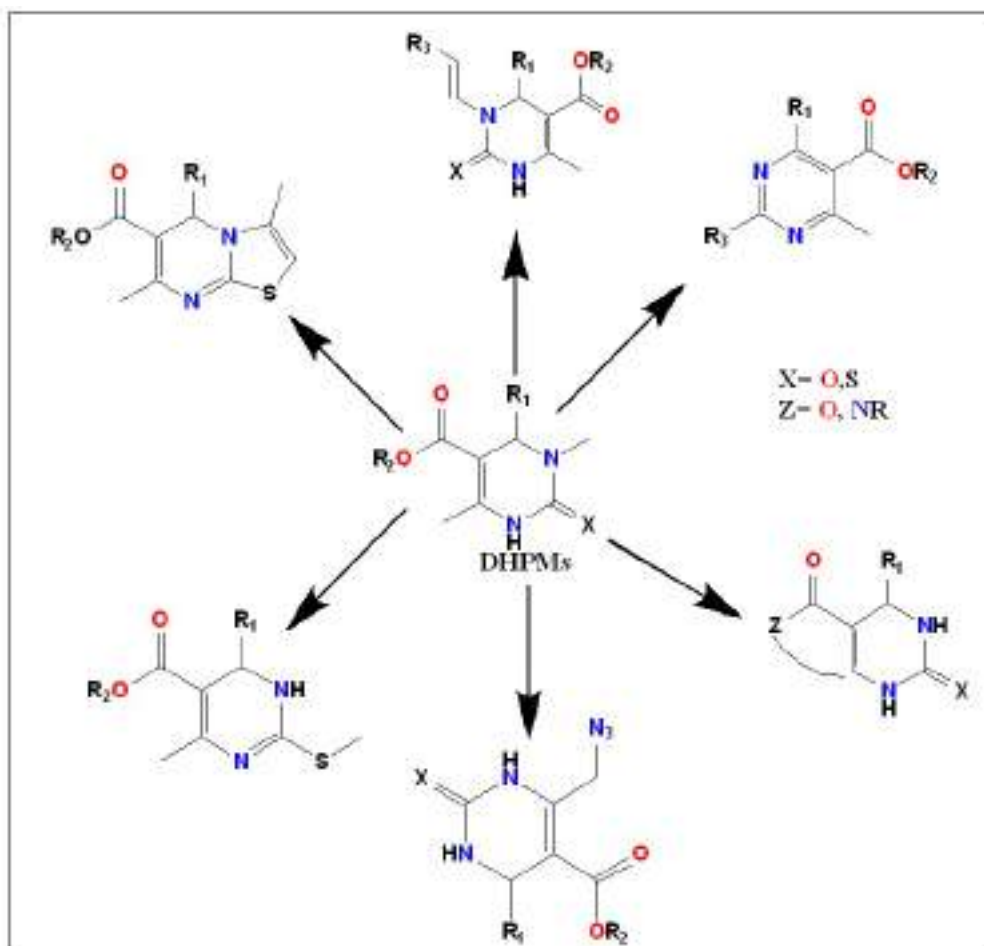


Fig. 4.B.1. DHPMs as essential building blocks.

Type 2 diabetes mellitus is a condition where regulation and use of glucose by the body is impaired leading to the increase of circulating blood sugar (when in the chronic stages). Eventually, disorders of the circulatory, immune and nervous systems. Type 2 diabetes is primarily the result of two correlated problems namely insulin resistance in cells in muscles, fat and liver causing reduced storage of glucose as glycogen, and the pancreas beta cells are unable to produce enough insulin to keep blood sugar levels in check²⁹. It is mostly characterized by hyperglycemia, insulin resistance and relative insulin deficiency³⁰. In the 2010s, inhibition of sodium-dependent glucose transporters (SGLTs) have been proposed as a new therapy for the treatment of type 2 diabetes mellitus³¹. SGLT2, the most prominent among all of the SGLTs, is expressed mainly in the kidney and is responsible for the reabsorption of a vast amount of the filtered glucose. Thus, SGLT2 plays a key role in the blood-glucose homeostasis and as such is a prominent target which has been clear from the results of pre-clinical and clinical studies. Any drug discovery project that focuses on promising SGLT2 inhibitors also has to factor in any significant selectivity towards SGLT1³². This is because though there are many therapeutic goals of SGLT2 inhibition like weight loss and

reduced plasma glucose levels, a few side effects may exist due to co-inhibition of SGLT1. SGLT1 being expressed in the intestine is responsible for glucose and galactose absorption from food sources, therefore, leading to galactose- and glucose malabsorption, diarrhoea and dehydration. This can be mediated through lack of selectivity towards SGLT1.

Selectivity of any drug or ligands towards SGLT2 thus needs to be offset by its lack of selectivity towards SGLT1. So, to describe selectivity with respect to structure, extensive use of molecular modelling techniques has been utilized as no x-ray structural data was available for either SGLT1 or SGLT2. Faham S. et al., thus, generated homology models for both transporters using the published x-ray structure from vSGLT (PDB 3DH4)³³. Although there are numerous drugs available for the treatment of type-2 diabetes mellitus still these drugs have several side effects³⁴. So, it is worthwhile to find an efficient drug for this disease with minimum or no side effect.

With the improvements in the field of drug designing, Molecular Docking studies are very popular in studying the different types of interactions between ligand and the receptor³⁵⁻³⁶.

Molecular docking is a virtual procedure which helps to find a ligand that fits exactly and efficiently in the binding site of the protein and is an important tool for accurate drug discovery³⁷⁻³⁸.

Furthermore, a variety of 2,4-dihydropyrimidin-2(1H)-ones using solvent free, green methodology have been prepared in excellent yields and its synthetic procedure, spectroscopic and analytical investigations have been discussed in section-A of chapter 4. In this chapter we are presenting the theoretical aspects of some selected Bigenelli compounds wherein HOMO-LUMO energies, bond lengths, bond angles, dihedral angles, global chemical descriptors and Molecular Electrostatic Potential (MEP) have been studied in detail using DFT. The inhibitory potential of these selected derivatives against the protein 3DH4 which is used in homology studies for the inhibition of Sodium-Dependent Glucose Transporters (SGLTs) have also been reported.

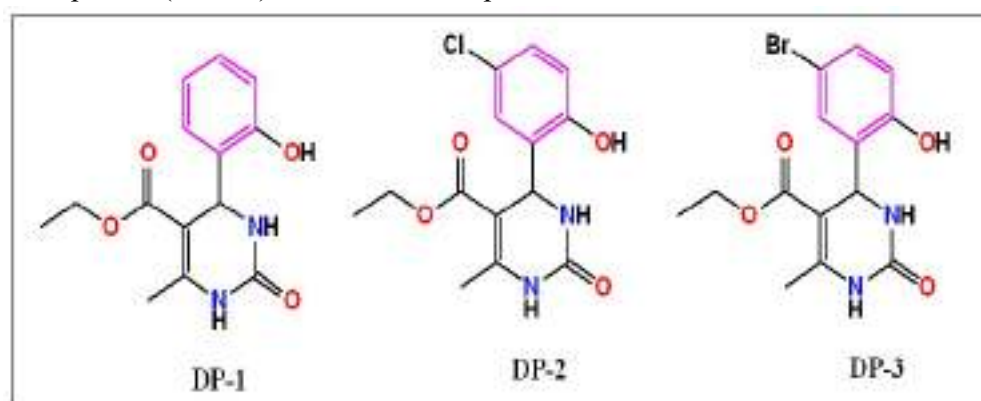


Fig. 4.B.2. Molecular Structures of selected 3, 4-dihydropyrimidin-(2H)-one derivatives (DP-1 to DP-3)

4.B.2 Results and Discussions

4.B.2.1 Computational Study

The molecular geometry, molecular orbital (HOMO,LUMO), Nonlinear Optical property (NLO), Global chemical descriptors and Molecular Electrostatic Potential (MEP) of the selected 3,4-dihydropyrimidin-(2H)-one derivatives namely, Ethyl 4-(2-hydroxyphenyl)-6-methyl-2-oxo-1,2,3,4-tetrahydropyrimidine-5-carboxylate (DP-1), Ethyl 4-(5-chloro-2-hydroxyphenyl)-6-methyl-2-oxo-1,2,3,4-tetrahydropyrimidine-5-carboxylate (DP-2) and Ethyl 4-(5-bromo-2-hydroxyphenyl)-6-methyl-2-oxo-1,2,3,4-tetrahydropyrimidine-5-carboxylate (DP-3) have been optimized by Density Functional Theory (DFT) using Becke's three-parameter hybrid method (B3) with Lee, Yang and Parr correlation functional methods (LYP) with B3LYP/631G+(d,2p) level of basis set³⁹⁻⁴⁰. All the computational calculations were calculated by Gaussian 16, Revision A.03 programme package⁴¹ and the results were visualized using GAUSSVIEW 6.0 software⁴² on ahp-Z640 desktop P.C. with an Intel Xeon processor (Specifications: E5-2630 V4 @ 220GHz).

4.B.2.1.1 Optimization of Molecular Geometry

To the best of our knowledge, the X-Ray single crystal structure of the selected compounds (DP-1 to DP-3) have not been reported till now, therefore, structure optimization using DFT method serves as a good alternative to ascertain the different geometrical parameters. The geometrical parameters of the studied compounds (DP-1 to DP-3) were calculated by DFT assay using B3LYP/631G+(d,2p) level of basis set. The optimized gas phase molecular geometry of the compounds (DP-1 to DP-3) with atom labelling scheme is shown in Fig.4.B.3 and 4.B.4 and the structural parameters like bond lengths, bond angles and dihedral angles are listed in Table 4.B.1.

From the analysis of the dihedral angles as given in Table 4.B.1, it can be inferred that the phenyl ring is not in plane with the DHPM nucleus as the dihedral angles are nowhere close to 0° or 180°. The dihedral angle between the phenyl ring (2) and the DHPM nucleus (1) depends on the type of substituent present in the phenyl ring as evident from the fact that in DP-1, the dihedral angle between C17-C12-C6-C5 and between C17-C12-C6-C1 is 34.148° and -138.05° respectively whereas in DP-2 it is -146.31° and 26.00° respectively and in DP-3 it is found to be 147.425° and -26.54° respectively. From Table 4.B.1, it is clearly seen that the C-N bond lengths in the DHPM nucleus (1) of all the studied compounds (DP-1 to DP-3) are in the range C6-N5 = 1.407 Å - 1.413 Å, C4-N5 = 1.370 Å - 1.377 Å, C4-N3 = 1.382 Å - 1.392 Å, C2-N3 = 1.393 Å - 1.401 Å respectively. The C4-N5 and C4-N3 are shorter than C6-N5 and C2-N3 a bond length which suggests that the lone pairs on nitrogen are delocalized on atom C4 which is double bonded with oxygen atom O19. Also, from the optimized geometry, it was found that C=O bond length in all the studied compounds (DP-1

to DP-4) fall in the range $C7=O8 = 1.210-1.219 \text{ \AA}$, $C4=O19 = 1.224-1.225 \text{ \AA}$ respectively. The C-O bond lengths in these compounds (DP-1 to DP-3) are found to be in the range $C7-O9 = 1.348-1.358 \text{ \AA}$, $C10-O9 = 1.450-1.455 \text{ \AA}$ respectively.

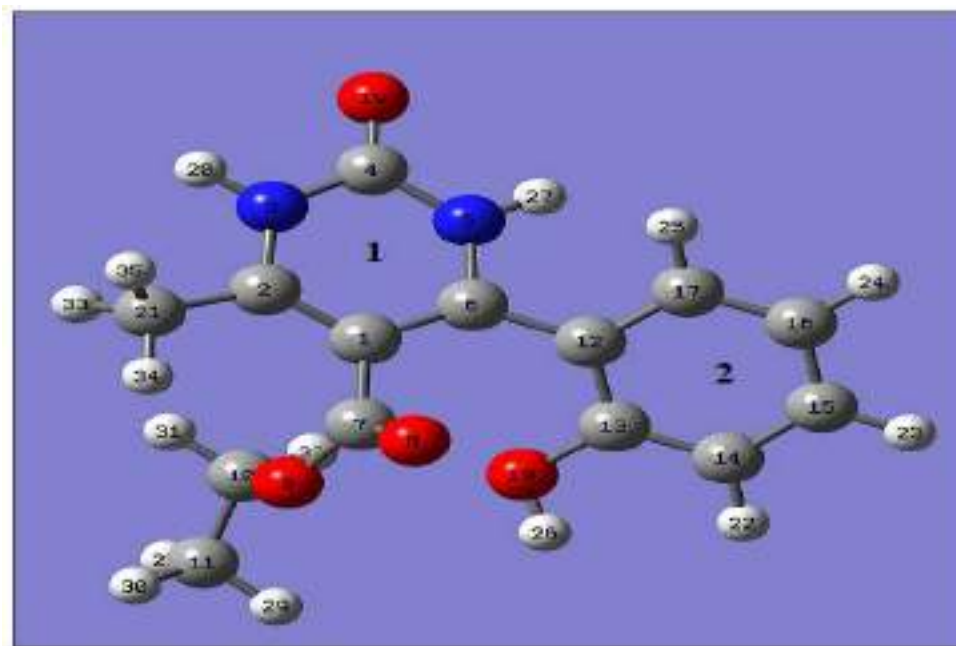


Fig. 4.B.3. Atom labelling of the DHPM nucleus (1) and the phenyl ring (2) in the studied compounds.

The C-C bond lengths of all the aryl groups present in the compounds (DP-1 to DP-3) are in the range 1.386 to 1.417 \AA which suggests that the carbon atoms are highly conjugated and electrons are involved in resonance⁴³. Again, from the table 4.B.1, it is clearly seen that the N-H bond length of the DHPM nucleus (1) in all the studied compounds are almost equal and falls in the range of $1.010-1.012 \text{ \AA}$. The aromatic C-H, aliphatic C-H, O-H, and C-halogen bond distances of the studied compounds (DP-1 to DP-3) are in the range $1.392-1.417 \text{ \AA}$, $1.086-1.094 \text{ \AA}$, $0.963-0.966 \text{ \AA}$, $1.761-1.909 \text{ \AA}$ respectively.

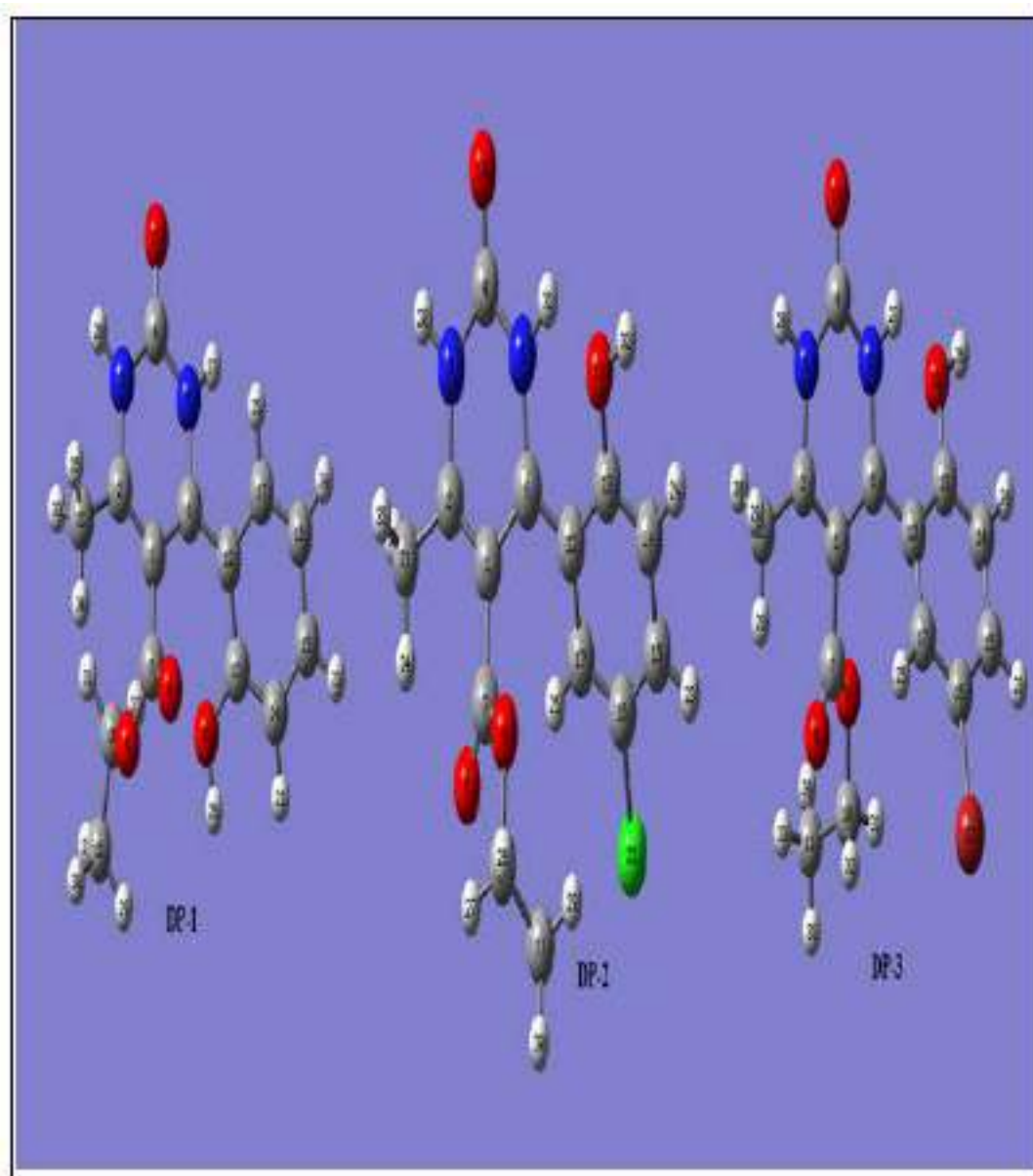


Fig. 4.B.4. Optimized gas phase molecular geometry of the compounds (DP-1 to DP-3) with atom labelling scheme.

Table. 4.B.1. Structural parameters (bond lengths, bond angles and dihedral angles) of the studied compounds (DP-1 to DP-3)

C-C bond length (Å)					
DP-1		DP-2		DP-3	
C2-C1	1.387	C2-C1	1.382	C2-C1	1.382
C6-C1	1.419	C6-C1	1.435	C6-C1	1.435
C6-C12	1.461	C6-C12	1.452	C6-C12	1.452
C7-C1	1.508	C7-C1	1.498	C7-C1	1.497
C11-C10	1.518	C11-C10	1.520	C11-C10	1.520
C12-C13	1.415	C12-C13	1.422	C12-C13	1.421
C12-C17	1.416	C12-C17	1.417	C12-C17	1.417
C13-C14	1.394	C13-C14	1.392	C13-C14	1.392
C14-C15	1.396	C14-C15	1.397	C14-C15	1.396
C15-C16	1.397	C15-C16	1.395	C15-C16	1.394
C16-C17	1.392	C16-C17	1.388	C16-C17	1.386
C2-C21	1.499	C2-C21	1.499	C2-C21	1.499
C-H, C-O, N-H, C-Cl, C-Br and O-H bond distances (Å)					
DP-1		DP-2		DP-3	
C10-H31	1.094	C10-H26	1.091	C10-H31	1.091
C10-H32	1.091	C10-H27	1.091	C10-H32	1.091
C11-H29	1.093	C11-H29	1.092	C11-H33	1.093
C11-H30	1.093	C11-H30	1.095	C11-H34	1.093
C11-H28	1.094	C11-H28	1.092	C11-H35	1.095
C14-H22	1.087	C14-H24	1.087	C14-H24	1.087
C15-H23	1.084	C15-H23	1.083	C15-H23	1.082
C16-H24	1.084	C17-H25	1.082	C17-H25	1.082
C17-H25	1.085	C21-H34	1.086	C21-H29	1.097
C21-H34	1.089	C21-H33	1.097	C21-H28	1.086
C21-H33	1.089	C31-H35	1.097	C21-H30	1.097
C21-H35	1.089	C4-O19	1.224	C7-O8	1.219
C7-O8	1.210	C7-O8	1.219	C7-O9	1.348
C10-O9	1.450	C10-O9	1.455	C10-O9	1.454
C7-O9	1.358	C7-O9	1.348	C4-O19	1.224
C13-O18	1.373	C13-O18	1.380	C13-O18	1.380
N3-H20	1.010	C16-Cl22	1.761	C16-Br22	1.909
N5-H27	1.010	N3-H20	1.010	N3-H20	1.010
		N5-H31	1.012	N5-H27	1.012
				O18-H26	0.965
Bond Angle (°)					
DP-1		DP-2		DP-3	
N3-C2-C1	118.536	N3-C2-C1	118.149	N3-C2-C1	118.168
C4-N3-C2	124.964	C4-N3-C2	124.805	C4-N3-C2	124.900
N5-C4-N3	113.609	N5-C4-N3	113.679	N5-C4-N3	113.724
C6-N5-C4	126.458	C6-N5-C4	125.653	C6-N5-C4	125.751
C7-C1-C2	117.987	C7-C1-C2	118.097	C7-C1-C2	118.307
O8-C7-C1	122.513	O8-C7-C1	124.954	O8-C7-C1	124.905
O9-C7-C1	118.270	O9-C7-C1	111.433	O9-C7-C1	111.501
C10-O9-C7	121.837	C10-O9-C7	117.416	C10-O9-C7	117.653
C11-C10-O9	107.199	C11-C10-O9	111.996	C11-C10-O9	110.810
C12-C6-N5	114.758	C12-C6-N5	118.386	C12-C6-N5	118.573
C13-C12-C6	123.601	C13-C12-C6	123.437	C13-C12-C6	123.612

C14-C13-C12	121.313	C14-C13-C12	121.406	C14-C13-C12	121.315
C15-C14-C13	120.635	C15-C14-C13	121.179	C15-C14-C13	121.185
C16-C15-C14	119.435	C16-C15-C14	118.164	C16-C15-C14	118.156
C17-C16-C15	119.776	C17-C16-C15	121.348	C17-C16-C15	121.344
O18-C13-C12	117.560	O18-C13-C12	117.857	O18-C13-C12	117.950
O19-C4-N3	122.986	O19-C4-N3	122.276	O19-C4-N3	122.260
H20-N3-C2	120.311	H20-N3-C2	119.635	H20-N3-C2	119.706
C21-C2-C1	127.084	C21-C2-C1	127.928	C21-C2-C10	127.915
H22-C14-C13	119.084	C122-C16-C15	119.316	Br22-C16-C1	119.423
H23-C15-C14	119.845	H23-C15-C14	120.889	H23-C15-C14	120.630
H24-C16-C15	120.450	H24-C14-C13	119.264	H24-C14-C13	119.247
H25-C17-C16	118.907	H25-C17-C16	118.859	H25-C17-C16	119.070
H26-O18-C13	109.471	H26-C10-O9	103.562	H26-O18-C13	109.820
H27-N5-C4	113.965	H27-C10-O9	108.559	H27-N5-C4	115.438
H28-C11-C10	109.660	H28-C11-C10	111.349	H28-C21-C2	111.974
H29-C11-C10	110.966	H29-C11-C10	111.087	H29-C21-C2	109.832
H30-C11-C10	110.980	H30-C11-C10	109.146	H30-C21-C2	110.311
H31-C10-O9	109.302	H31-N5-C4	115.525	H31-C10-O9	104.054
H32-C10-O9	109.177	H32-O18-C13	109.866	H32-C10-O9	108.843
H33-C21-C2	111.242	H33-C21-C2	109.785	H33-C11-C10	110.970
H34-C21-C2	112.093	H34-C21-C2	111.958	H34-C11-C10	110.911
H35-C21-C2	110.254	H35-C21-C2	110.351	H35-C11-C10	109.565
Selected dihedral angles (°)					
C17-C12-C6-C5	34.140	C17-C12-C6-C5	-146.301	C17-C12-C6-C5	147.420
C13-C12-C6-C1	45.550	C13-C12-C6-C1	-156.009	C13-C12-C6-C1	154.530
C13-C12-C6-C5	-144.240	C13-C12-C6-C5	31.570	C13-C12-C6-C5	-31.500
C1-C6-C12-C17	-138.050	C1-C6-C12-C17	26.000	C1-C6-C12-C17	-26.540
O8-C7-C1-C6	60.470	O8-C7-C1-C6	-138.601	O8-C7-C1-C6	138.760
C2-C1-C7-O8	-109.610	C2-C1-C7-O8	48.060	C2-C1-C7-O8	-46.580
H31-C10-C11-H29	179.310	H27-C10-C11-H29	177.980	H32-C10-C11-H33	56.640
H31-C10-C11-H30	-60.200	H27-C10-C11-H30	-62.680	H31-C10-C11-H33	179.400
O9-C10-C11-H30	58.910	O9-C10-C11-H30	175.450	O9-C10-C11-H33	-65.160

O9-C10-C11- H29	-61.510	O9-C10-C11- H29	56.130	O9-C10-C11- H35	179.500
C2-C1-C7- O9	66.010	C2-C1-C7-O9	-128.907	C2-C1-C7-O9	131.950

4.B.2.1.2 Frontier Molecular Orbitals

The Highest occupied molecular orbital (HOMO) and the Lowest Unoccupied Molecular orbital (LUMO) constitutes the frontier molecular orbitals and they are very important in predicting the molecular reactivity. The electron donor ability of a molecule is determined by the energy of HOMO while the electron acceptor ability is determined by the energy of LUMO⁴⁴. Several important properties like kinetic stability, reactivity and the polarizability of a molecule can be determined by analyzing the energy gap ($\Delta E = E_{\text{LUMO}} - E_{\text{HOMO}}$) between the HOMO and the LUMO⁴⁴. Also, a large and positive ΔE value indicates that the molecule is less polarizable and is chemically stable⁴⁵. In order to get into a deep insight into the electronic behavior of the studied compounds, the HOMO-LUMO energies have been calculated using B3LYP/631G+(d,2p) basis set and its pictorial representation is shown in Fig.4.B.5. and the energies of the HOMO-LUMO of the studied compounds are shown in Table 4.B.2.

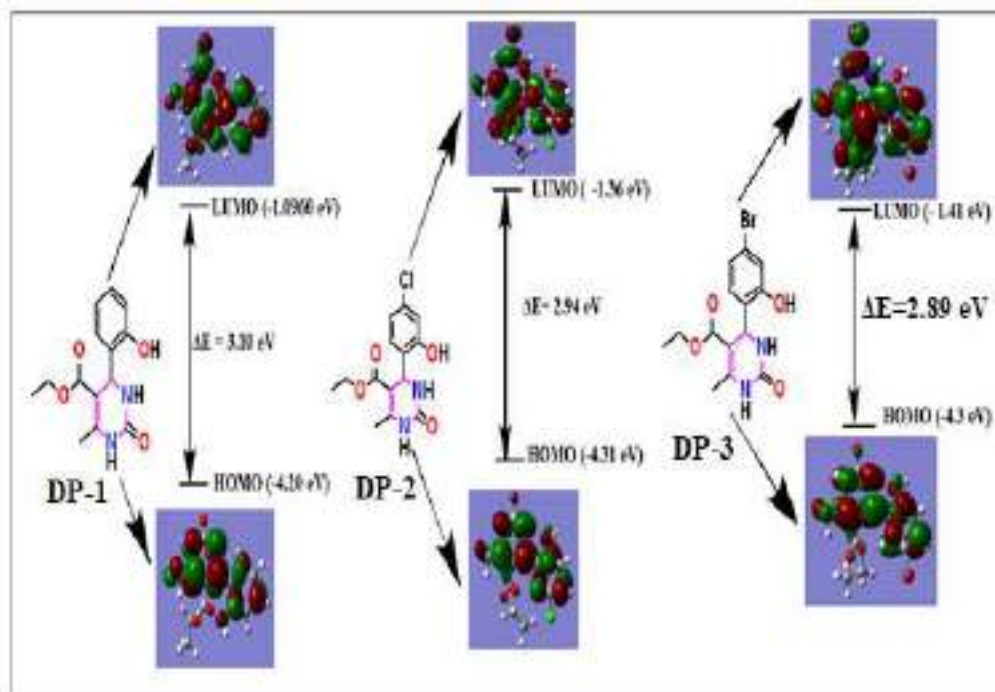


Fig. 4.B.5. Pictorial representation of the HOMO-LUMO of selected compounds (DP-1 to DP-3)

From the Table 4.B.2., It is evident that the energy of HOMO and LUMO orbitals are negative and this shows that the compounds under study (DP1 to DP-3) are relatively stable⁴⁵ and the energy of HOMO and LUMO orbitals of the compounds are -4.20 eV (DP-1), -4.31 eV (DP-2), -4.30 eV (DP-3) and -1.09 eV (DP-1), -1.36 eV (DP-2), -1.41 eV (DP-3) respectively. With the help of the energies of the HOMO and LUMO, global chemical descriptors like chemical potential, global hardness and global electrophilicity can be determined which is helpful for understanding the reactivity and the structure of the molecule which in turn is essential for determination of the various pharmacological properties of the molecule for the process of drug design⁴⁶. The ionization energy (I) and electron affinity (A) can be expressed in terms of HOMO and LUMO orbital energies as follows

$$I = -E_{\text{HOMO}} \text{ and } A = -E_{\text{LUMO}}$$

The chemical reactivity descriptors such as chemical potential (μ), Electronegativity (χ), Global hardness (η) and global electrophilicity power (ω) can be calculated with the help of following relation;

$$\text{Chemical potential } (\mu) = (E_{\text{HOMO}} + E_{\text{LUMO}})/2 = -(I+A)/2$$

$$\text{Electronegativity } (\chi) = (I+A)/2$$

$$\text{Global Hardness } (\eta) = (-E_{\text{HOMO}} - E_{\text{LUMO}})/2 = (I-A)/2$$

$$\text{Electrophilicity power } (\omega) = \mu^2/2 \eta$$

Where I and A are the first ionization potential and electron affinity of the chemical species⁴⁷⁻⁴⁹.

The ionization energy (I), electron affinity (A), Chemical potential (μ), Electronegativity (χ), Global hardness (η) and Global electrophilicity power (ω) of the studied compounds (DP-1 to DP-3) are listed in Table 4.B.3.

Table. 4.B.2. Energies of HOMO and LUMO orbitals, ionization energy (I), electron affinity (A), Chemical potential (μ), Electronegativity (χ), Global hardness (η) and Global electrophilicity power (ω) of the studied compounds (DP-1 to DP-3)

Parameters (eV)	DP-1	DP-2	DP-3
E_{HOMO}	-4.20	-4.31	-4.30
E_{LUMO}	-1.09	-1.36	-1.41
ΔE	3.10	2.94	2.89
Ionization Energy (I)	4.20	4.31	4.30
Electron Affinity (A)	1.09	1.36	1.41
Chemical potential (μ)	-2.64	-2.83	-2.85
Electronegativity (χ)	2.64	2.83	2.85
Global hardness(η)	1.55	1.47	1.44
Electrophilicity power(ω)	2.25	2.72	3.81

It is seen that the chemical potential of all the studied molecules are negative and this suggests that the compounds under investigation do not decompose spontaneously into its elements they are made up of.

Apparently, it is seen that the hard molecule has large HOMO-LUMO gap and soft molecule has small HOMO-LUMO gap⁵⁰. Thus, from the Table 4.B.3, it is evident that the hardness of the studied molecule follows the order DP-1 > DP-2 > DP-3. Moreover, the hardness signifies the resistance towards the deformation of electron cloud of chemical systems under small perturbation that occur during the chemical reaction. Thus, hard system is less polarizable than soft system⁵¹. Again, a large value of electrophilicity is assigned for good electrophile whereas nucleophile is described by low value of nucleophilicity⁵².

4.B.2.1.3 FT-IR analysis

Study of the molecular vibrations of organic compounds is an important area of research as it is possible to correlate the theoretical and experimental FT-IR spectra of the studied compounds to figure out the different structural features in the molecules.

The theoretical vibrational spectra of the studied compounds (DP-1 to DP-3) was calculated using B3LYP/631G+(d,2p) basis set on the optimized geometry of the molecules in the gas phase. The experimental and theoretical vibrational

frequencies of the studied compounds (DP-1 to DP-3) are given in Table 4.B.3 with proper assignment of the observed peaks.

Table. 4.B.3. FT-IR analysis of studied compounds DP-1 to DP-3

DP-1				
Unscaled frequency (cm-1) (theoretical)	IR _i	R(A)	IR Frequency (cm-1) Experimental	Assignments
3821.74	69.7539	96.4066	3444	vOH stretch
3639.2	96.5826	232.3846	3009	vNH stretch
3626.02	40.3333	94.4064		vNH stretch
3209.13	14.3066	301.7885		v(s)Ar-H stretch
3195.6	9.456	75.1909		v(as)Ar-H stretch
3183.72	2.6979	58.8911		v(as)Ar-H stretch
3162.77	12.7405	107.6511		v(as)Ar-H stretch
3155.52	2.4726	43.1897		v(as)CH ₃
3133.24	25.3587	5.5061		v(as)C ₂ H ₅
3115.21	23.2341	65.8397		v(as)C ₂ H ₅
3110.33	1.6272	86.7641		v(as)C ₂ H ₅
3058.58	22.7075	88.3833		v(as)C ₂ H ₅
3045.41	7.9017	262.1293	2988	vC ₂ H ₅ ,v(as)CH 3
3045.06	32.4389	163.6919		vC ₂ H ₅ ,v(as)CH 3
3006.11	87.5886	680.6065		vCH ₃
1637	14.539	1000.461		vAr C=C stretch, 1
1615.03	31.014	67.1562	1629	vAr C=C stretch
1555.13	59.3641	259.6895	1531	vArC=C stretch
1790.21	1074.1713	36.4448	1666	v(C=O) stretch
DP-2				
3826.93	89.3908	147.631		vOH
3632.99	116.8733	247.8722	3444	vNH
3595.47	87.0333	115.2456		vNH
3223.96	0.1725	113.6372		vAr-H
3220.11	0.1289	14.8199		v(as)Ar-H
3188.08	0.7012	37.0334		v(as)CH ₃
3164.66	16.1413	162.2694		v(as)Ar-H
3145.92	17.4996	4.2482		v(as)C ₂ H ₅
3124.08	3.3019	72.0917		v(as)C ₂ H ₅
3114.24	31.4035	80.5211		v(as)C ₂ H ₅
3079.04	29.1354	115.075		v(as)C ₂ H ₅

3061.2	12.2927	219.1467		v(as)CH ₃
3047.06	14.3386	183.7124		vC ₂ H ₅
3017.79	73.4512	739.7649	3004	vCH ₃
1622.84	1070.0928	1178.464		vArC=C stretch
		9		
1601.41	50.1923	258.3946	1625	vAr C=C stretch
1587.72	123.0225	301.1709		vAr C=C stretch
1790.76	1013.8192	42.7887	1667	vC=O stretch
DP-3				
3826.49	90.5042	152.7938	3473	vOH
3633.14	120.0181	261.1812	3455	vNH
3596.46	86.4332	124.2294		vNH
3223.38	0.6732	98.986		vAr-H
3220.45	0.3245	10.9341		v(as)Ar-H
3188.57	0.6232	37.27		v(as)CH ₃
3163.85	16.7887	168.0818		v(as)Ar-H
3144.92	13.6097	6.3731		v(as)C ₂ H ₅
3119.59	9.7442	56.2076		v(as)C ₂ H ₅
3111.15	20.7016	85.4523		v(as)C ₂ H ₅
3060.74	12.4734	222.5195		v(as)CH ₃
3043.58	20.9182	168.1723		vC ₂ H ₅
3017.63	74.5452	745.067	2969	vCH ₃
1621.72	106.7411	1271.234		vArC=C stretch
		5		
1599.92	61.0917	271.8334		vAr C=C stretch
1586.55	113.1961	310.4236	1474	vAr C=C stretch
1791.55	1035.7274	1791.55	1635	v(C=O) stretch

4.B.2.1.3.1 C-H stretching vibration

For the studied compounds (DP-1 to DP-3), C-H functional group is present at various positions. The characteristic C-H stretching vibration of the aromatic ring falls in the range 3100-3000 cm^{-1} ⁵³. In the present investigation, theoretically calculated bands in the range of 3209-3162 cm^{-1} , 3223-3164 cm^{-1} and 3220-3163 cm^{-1} were assigned to aromatic C-H stretching vibrations for the compounds DP-1, DP-2 and DP-3 respectively. Pure symmetric bands were calculated at 3209 cm^{-1} in DP-1, 3223 cm^{-1} in DP-2 and 3223 cm^{-1} in DP-3 respectively. Asymmetric vibrational bands were calculated with stretching frequencies 3195 cm^{-1} , 3183 cm^{-1} and 3162 cm^{-1} for DP-1, 3220 cm^{-1} , 3220 cm^{-1} , 3164 cm^{-1} for DP-2 and 3220 cm^{-1} , 3163 cm^{-1} for DP-3 respectively. Because of the integration of several bands in the molecules, it is very difficult to detect the aromatic C-H stretching in this type of systems.

The characteristic C-H stretching vibration for aliphatic systems like the C-H symmetric stretching vibration for CH₃ group is found at 3006 cm⁻¹ for DP-1, 3017 cm⁻¹ for DP-2 and 3017 cm⁻¹ for DP-3 respectively. The experimentally observed values for C-H symmetric stretching vibrations for CH₃ group lies in the range 2988 cm⁻¹ for DP-1, 3004 cm⁻¹ for DP-2 and 2969 cm⁻¹ for DP-3 respectively. Another important C-H stretching vibration found in BHPMs is the C-H symmetric stretching vibration for C₂H₅ group. Theoretically, the C-H symmetric stretching vibration for C₂H₅ group is found at 3045 cm⁻¹ for DP-1, 3047 cm⁻¹ for DP-2 and 3043 cm⁻¹ for DP-3 respectively.

4.B.2.1.3.2 C-O stretching vibration

For the studied compounds, the C=O stretching frequency is an important stretching vibration. The C=O stretching vibration for the studied compounds were found at 1790.21 cm⁻¹ for DP-1, 1790.76 cm⁻¹ for DP-2 and 1791.55 cm⁻¹ for DP-3 respectively. The experimental C=O stretching vibration for these compounds were found at 1666 cm⁻¹ for DP-1, 1667 cm⁻¹ for DP-2 and 1635 cm⁻¹ for DP-3.

4.B.2.1.3.3. N-H stretching vibration

N-H stretching vibration is an important stretching vibration for the studied compounds (DP-1 to DP-3). For the compound DP-1, the theoretical N-H stretching vibration was found at 3639 cm⁻¹, for DP-2 it was found at 3632 cm⁻¹ and for DP-3 it was found at 3633 cm⁻¹. The experimentally determined N-H stretching vibration for DP-1 was assigned at 3009 cm⁻¹, for DP-2 it was found at 3444 cm⁻¹ and for DP-3 the N-H stretching vibration was found at 3455 cm⁻¹ respectively.

4.B.2.1.3.4. Aromatic C-C stretching vibration

Generally, the bands observed in the range 1650-1400 cm⁻¹ are assigned to C-C stretching mode of aromatic derivatives⁵⁴. In our present study, the range for theoretically calculated C-C stretching vibrational mode showing sharp bands are in the range 1637-1555 cm⁻¹, 1622-1587cm⁻¹ and 1621-1586 cm⁻¹ for DP-1, DP-2 and DP-3 respectively (Table 4.B.3). Experimentally, the aromatic C-C stretching frequencies for the studied compounds observed in the range 1629-1531 cm⁻¹ in DP-1, 1625 cm⁻¹ in DP-2, and 1474 cm⁻¹ for DP-3 respectively.

Thus, from the above discussions, it is evident that the theoretically calculated vibrational frequency matched well with the experimental results for the studied compounds (Fig. 4.B.6).

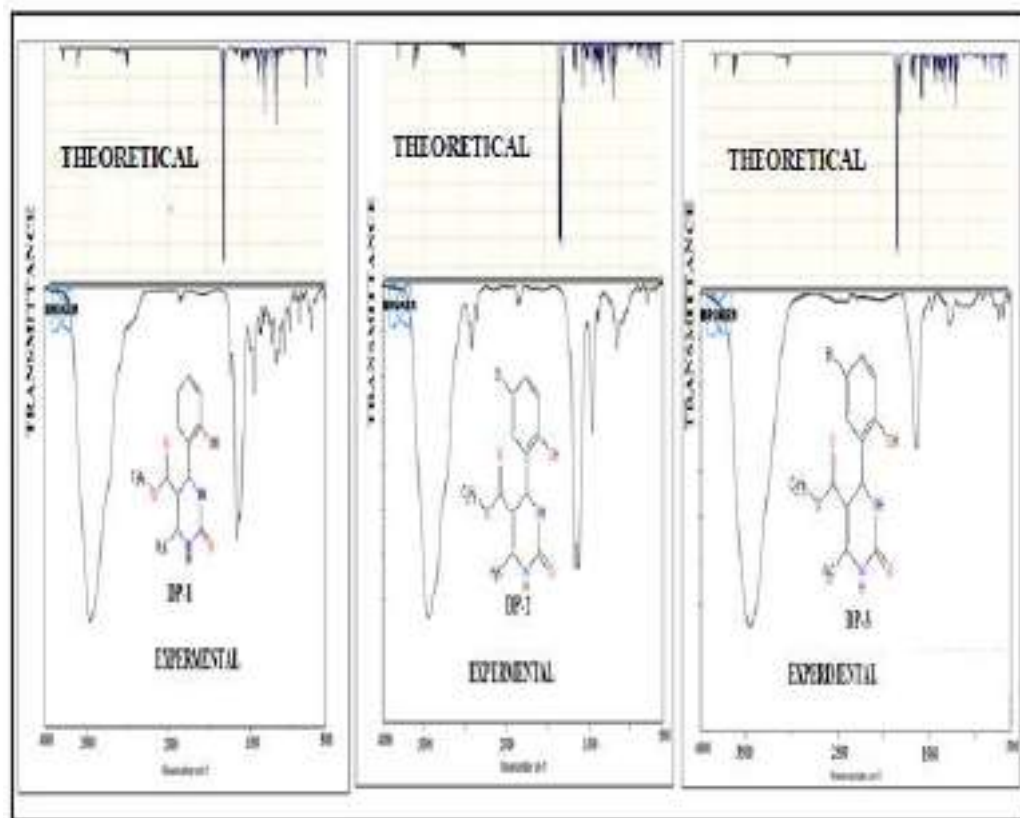


Fig. 4.B.6. Theoretical and experimental FTIR spectra of DP-1 to DP-3

4. B.2.1.4 Molecular Electrostatic Potential (MEP)

In chemical systems, the electrostatic potential around molecules is an important parameter for assessing and correlating the molecular structure and their physicochemical properties⁵⁵. Moreover, MEP helps in understanding the sites of electrophilic and nucleophilic reactions, along with hydrogen bonding interactions⁵⁶. To analyze the reactive sites of electrophilic and nucleophilic attack for the compounds under study (DP-1 to DP-3), Molecular Electrostatic Potentials at B3LYP/631G+ (d, 2p) was calculated. The electrostatic potentials at the MEP surfaces are given by different colors like red, blue and green. Red, blue and green colour represents the region of most negative, most positive and zero electrostatic potential respectively. Thus, the electrostatic potential increases in the order blue > green > yellow > orange > red. The most negative electrostatic potential (red, orange and yellow region) in the MEP surface is assigned for the electrophilic reaction sites and the positive (blue) region corresponds to nucleophilic reaction site⁵⁷⁻⁵⁸. The MEP surface of the studied compounds (DP-1 to DP-3) is depicted in Fig.4.B.7. A detailed description of the MEP surface indicating the region of negative/ electrophilic reaction sites and positive/nucleophilic reaction site for the studied compounds (DP-1 to DP-3) are listed in Table 4.B.4.

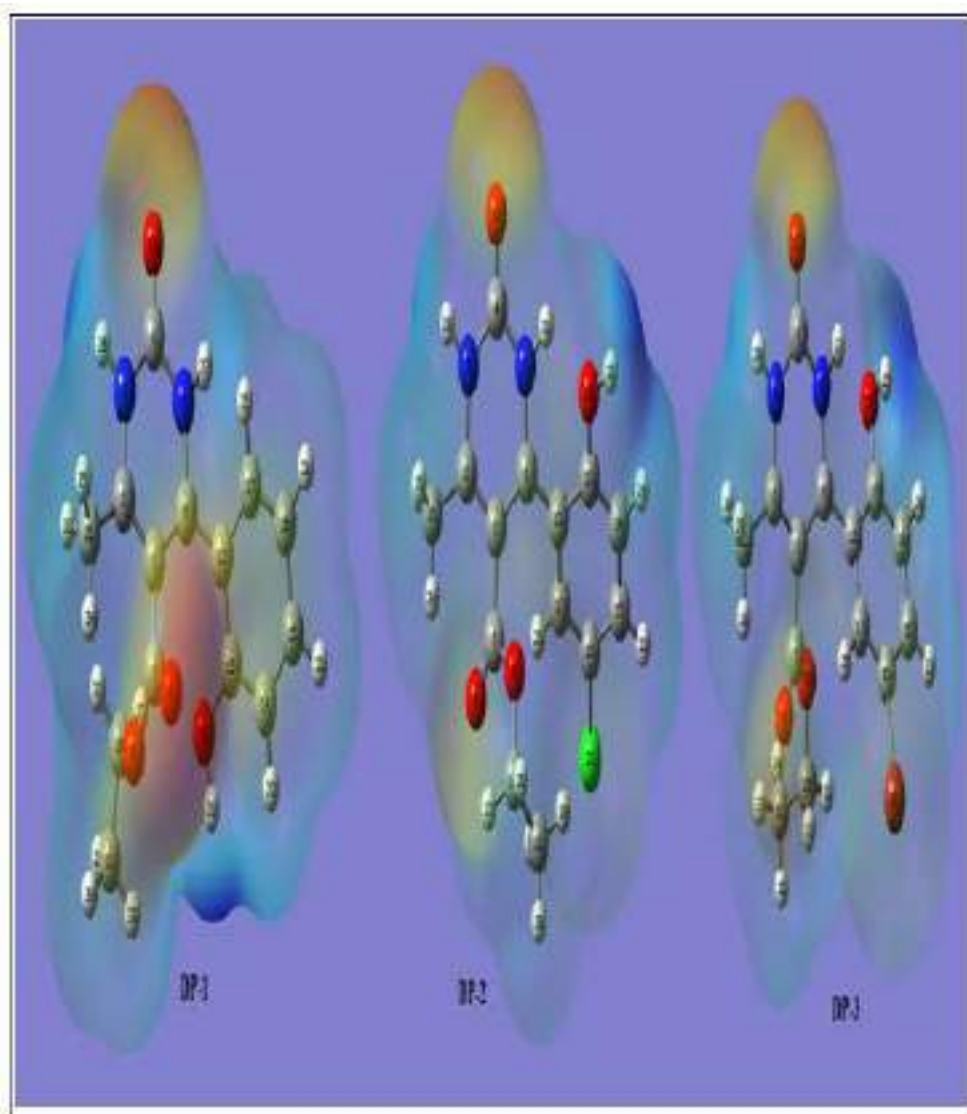
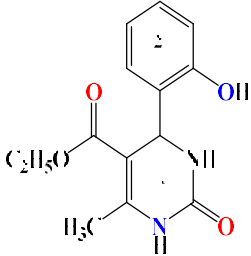


Fig. 4.B.7. MEP plots of studied compounds (DP-1 to DP-3)

Table. 4.B.4. Detailed description of MEP surface for compounds DP-1 to DP-3

Entry	Negative region (red, orange, yellow)/Electrophilic reaction site	Positive region (blue)/ Nucleophilic reaction site
	DP-1	-OH group of 2-phenyl ring and O19,O8,O9 of the DHPM nucleus 1
	DP-2	N5-H27(1), N3-H20(1), H26 of the DHPM nucleus (1) and H26 of the phenyl ring 2
	DP-3	O19, O8 of DHPM nucleus1
	DP-3	N3-H20, C21-H28,H29,H30, of DHPM nucleus1 and -O18H25 group of phenyl ring2

4.B.2.1.2.5 NLO properties

Nonlinear optical phenomenon is generally caused by the interaction of materials with electromagnetic fields, resulting in altered wave numbers, phases, or other physical properties of the electromagnetic field⁵⁹. Organic molecules having extended π - conjugation with delocalized electrons and intra molecular charge transfer from donor to acceptor orbital through π -spacer generally show a rapid response to light and have strong NLO properties⁶⁰. Organic molecules having good non-linear properties are widely used in the field of organic light emitting diodes, transistors and dye sensitized solar cells⁶¹

Theoretically, the NLO properties of the given compound is calculated by determining the parameters such as magnitude of dipole moment (μ), polarizability (α), anisotropy of polarizability ($\Delta\alpha$), first hyperpolarizability (β) and second order hyperpolarizability (γ). The polarizability tensors are calculated using the following relations⁶²

$$\text{Dipole moment } \mu = (\mu_x^2 + \mu_y^2 + \mu_z^2)^{1/2} \dots\dots\dots (1)$$

$$\alpha(\text{total}) \text{ or } \langle \alpha \rangle = \frac{1}{3} (\alpha_{xx} + \alpha_{yy} + \alpha_{zz}) \dots\dots\dots (2)$$

$$\Delta\alpha = 1/\sqrt{2} [(\alpha_{xx} - \alpha_{yy})^2 + (\alpha_{yy} - \alpha_{zz})^2 + (\alpha_{zz} - \alpha_{xx})^2 + 6(\alpha_{xy}^2 + \alpha_{xz}^2 + \alpha_{yz}^2)]^{1/2} \dots\dots\dots (3)$$

$$\beta_x = \beta_{xxx} + \beta_{xyy} + \beta_{xzz} \dots\dots\dots (4)$$

$$\beta_y = \beta_{yyy} + \beta_{yzz} + \beta_{yxx} \dots\dots\dots (5)$$

$$\beta_z = \beta_{zzz} + \beta_{zxx} + \beta_{yyz} \dots\dots\dots (6)$$

$$\beta_{\text{total}} = (\beta_x^2 + \beta_y^2 + \beta_z^2)^{1/2} \dots\dots\dots (7)$$

$$\langle \gamma \rangle \text{ or } \gamma_{\text{total}} = 1/5 (\gamma_{xxxx} + \gamma_{yyyy} + \gamma_{zzzz} + 2(\gamma_{xxyy} + \gamma_{yyzz} + \gamma_{xxzz})) \dots\dots\dots (8)$$

The nonlinear optical properties such as dipole moments, dipole polarizabilities, first- and second order hyperpolarizabilities of the studied compounds (DP-1 to DP-3) were calculated by B3LYP/ 6-31G + (d, 2p) basis set and the computed results are listed in Table 4.B.5.

Table. 4.B.5. Computed Dipole moments, dipole polarizabilities and anisotropic Polarizabilities and first-order hyperpolarizabilities of compounds DP-1 to DP-3

Dipole moments, dipole polarizabilities and anisotropic polarizabilities				
Entry	DP-1	DP-2	DP-3	Ref.
μ_x	-1.1327	-3.0611	0.2975	0
μ_y	-2.6007	0.1471	2.6826	-4.06
μ_z	-2.1905	-0.3033	-0.3464	0.0018
μ	3.5840	3.0796	2.7212	4.06
α_{xx}	-94.9715	-149.803	-159.27	-16.62
α_{yy}	-126.959	-106.795	-109.169	-24.64
α_{zz}	-127.257	-134.888	-140.665	-27.03
α_{xy}	-1.4797	18.461	15.8639	-0.0003
α_{xz}	-1.4248	0.4048	-0.0525	-0.07
α_{yz}	15.2026	-1.4331	-1.5948	0.01
$\alpha_{tot} \times 10^{-24}(\text{esu})$	-17.249	-19.266	-20.209	-3.37
$\Delta\alpha \times 10^{-24} (\text{esu})$	6.179	7.350	7.681	1.39
First order hyperpolarizabilities				
β_{xxx}	-26.36	-68.10	-157.70	-0.002
β_{xyy}	25.66	-42.54	-48.73	-0.0004
β_{xzz}	-16.98	3.72	-28.344	0.001
β_{yyy}	-125.62	-77.15	-51.36	-16.94
β_{xxy}	3.44	73.77	98.76	-0.63
β_{yzz}	2.49	8.88	12.02	2.05
β_{zzz}	-14.93	-1.43	-4.43	-0.01
β_{xxz}	8.75	-4.99	-4.12	-0.09
β_{yyz}	7.03	-1.69	-1.51	-0.03
β_{xyz}	-10.75	4.48	2.97	0.05
$\beta_{total} \times 10^{-30}$ (esu)	1.045	0.927	2.094	0.13

A comparative study of the dipole moment in the studied system indicates that they have different charge distributions for different directions. The theoretically calculated dipole moments of the studied compounds are 3.58D (DP-1), 3.079D (DP-2), 2.721D (DP-3) respectively and the dipole moment follows the order DP-1 > DP-2 > DP-3.

The compounds DP-1, DP-2 and DP-3 have dipole moment value less than the dipole moment value of urea (4.06 D) reference. Also, the total dipole polarizabilities value of the studied compounds along all three directions is listed in Table 4.B.5. From the Table 4.B.5, it is evident that the dipole polarizability of the studied compounds follows the order DP-3(-20.209×10^{-24}) > DP-2(-19.266×10^{-24}) > DP-1(-17.249×10^{-24}).

The theoretically computed first-order hyperpolarizabilities and their individual components for the studied compounds (DP-1 to DP-3) are listed in Table 4.B.6. From the Table 4.B.5, it is evident that the first-order hyperpolarizability of the studied compounds are 1.045×10^{-30} esu, 0.927×10^{-30} esu and 2.094×10^{-30} esu for compounds DP-1, DP-2 and DP-3 respectively. A comparison of the first-order hyperpolarizability value of the studied compounds with the standard reference urea (0.13×10^{-30} esu) have shown that the studied compounds have far greater value of first-order hyperpolarizability value than urea. Thus, the order for the first-order hyperpolarizability of the studied compounds are DP-3 > DP-1 > DP-2.

The second order hyperpolarizabilities of the compounds DP-1 to DP-3 are given in Table 4.B.6. The second order hyperpolarizability of the studied compounds are -0.877×10^{-36} esu, -1.129×10^{-36} esu and -1.670×10^{-36} esu for DP-1, DP-2 and DP-3 respectively.

Table. 4.B.6. Second order hyperpolarizabilities of studied compounds DP-1 to DP-3

Second order hyperpolarizabilities							
Entry	γ_{xxxx}	γ_{yyyy}	γ_{zzzz}	γ_{xxyy}	γ_{yyzz}	γ_{xxzz}	γ_{total} (x 10^{-36}) esu
DP-1	-3558.66	-3133.59	-635.75	-86.88	174.92	-779.3	-0.87
DP-2	-5633.49	-3064.38	-191.64	443.58	-680.33	-924.5	-1.12
DP-3	-6568.69	-3064.22	-201.93	-1639.22	-683.36	-1050	-1.67
Urea	-120.66	-117.90	-29.39	-44.02	-28.01	-39.86	-0.04

The order of second-hyperpolarizability of the studied compounds is given by DP-3 > DP-2 > DP-1 and from the Table 4.B.6, it is evident that the second-order

hyperpolarizability of the studied compounds are much greater than the reference NLO material urea.

From the above discussion, it is evident that the studied molecule DP-1 to DP-3 have shown greater value of nonlinear optical parameters than the reference urea molecule and we may infer that this set of molecules could act as a better nonlinear optical material.

4.B.2.2 Molecular Docking Study

Type-2 diabetes mellitus is a condition where there is an elevation of glucose level in the blood (hyperglycemia) or an elevation in the insulin levels in the blood (hyperinsulinemia)⁶³. Among various available therapies for type-2 diabetes mellitus, Sodium glucose co-transporter 2 (SGLT2) inhibitors are very popular class of drugs which is used to control hyperglycemia⁶⁴

Molecular Docking studies now days have become an essential tool for drug design and provides helpful information about various interactions between the ligand and the protein in a faster and cost-effective way^{62,65}. In this chapter, we have reported the molecular docking study of the selected 3,4 Dihydropyrimidine-2-[1H]-one derivatives against the protein 3DH4.

The protein 3DH4 structure has often been used in homology studies for the inhibition of sodium-dependent glucose transporters (SGLTs). The protein has an approximately 3.0 Å structure that contains 14 transmembrane helices in an inward facing conformation with a core structure of inverted repeats of 5 TM helices (TM2 – TM6 and TM7 – TM11). Galactose can be found bound to the center of the core, kept in place away from the outside by hydrophobic residues.

4.B.2.2.1 Visualization of the Docking Result

Molecular docking study of the compounds (DP-1 to DP-3) against the protein 3DH4 has been carried out using GUI interface programme of Autodock Tools (MGL tool or Molecular Graphics Laboratory tool developed by Scripps research Institute⁶⁶. The docking results have been visualized with the help of Biovia Discovery Studio 2020 (DS), version 21.1.0.20298 and Edu Pymol version 2.5.2.

After successful docking of the compounds (DP-1 to DP-3) with the protein 3DH4, the docking result showed different types of protein-ligand interactions with particular binding energies. For better understanding of fitting of the ligand into the binding pocket of the protein, ligands are shown as blue green stick. The hydrogen bonding interactions between ligands and protein are shown by green dash line, the π -sulfur interaction as yellow dash line, π -anion/ π -cation interactions as orange dash line, π -sigma interactions as purple dash line, π - π stacking/ π - π T-shaped interactions as dark pink dash line and π -alkyl interactions as light pink dash line respectively. The binding energy (ΔG) and the predicted inhibitory constant (pK_i) of the studied compounds (DP-1 to DP-3) are found to be -6.9 Kcal/mole (DP-1), -

7.9 Kcal/mole (DP-2), -6.1 Kcal/mole (DP-3) respectively and 6.85 μM , 1.23 μM , and 27.22 μM respectively (Table 4.B.7)

Table. 4.B.7. Summary of docking of the compound (IM-1 to IM-6) against insulin receptor protein IIR3 with corresponding binding energy (ΔG), predicted inhibitory constant (pK_i), interacting amino acid residues and type of interactions.

Ligands	Binding Energy (kcal/mol)	Predicted inhibitory constant (pK_i) μM	Amino Acid residues	Types of interactions
DP-1	-6.9	6.85	Phe133, Tyr430, Leu433, Ile464, Val434	π - π T-shaped, Alkyl, π - Alkyl π -Sigma
DP-2	-7.9	1.23	Phe479, Met244, Met477, Lys471	Conventional H-bonding, Unfavorable Acceptor-Acceptor, π -Donor Hydrogen Bond, Carbon H-bond
DP-3	-6.1	27.22	Glu68, Gln69, Asn142, Asn267, Leu137, Tyr263	Conventional H-bonding Alkyl, π - Alkyl, Halogen (Cl, Br)

The visualization of the docking result of compound DP-1 with the protein 3DH4 showed that the ligand fits into a pocket region present in the outer regions of the protein surface (Fig. 4.B.7). A close analysis of the docking result revealed that the ligand interacts with the protein with binding energy (ΔG) value of -6.9 Kcal/mole and predicted inhibitory constant (pK_i) 6.85 μM . The main interactions between the ligand DP1 and the protein were characterized by different interactions between π – electron of the ligand and different amino acid residues. A π - π T-shaped interaction is observed between the phenyl ring of the amino acid residue Phe133 and the phenyl ring of the ligand DP-1 at a distance of 5.00 Å. A π -sigma interaction occurs between the sigma electron of isopropyl group of amino acid residue Val434 and π -electron of the phenyl ring of the ligand DP-1 at a distance 3.80 Å. In addition, there are three π -alkyl interactions also observed between the ligand DP-1 and the protein. The first and second π -alkyl interactions exist between the π -electron of the phenyl ring of ligand DP-1 and alkyl group of amino acid residue Ile464 and Leu433 at 5.09 Å and 5.32 Å respectively. The third π -alkyl interaction was observed between the CH_3 (6) group of the ligand DP-1 and the π -electron of phenyl ring of amino acid residue Tyr430 at 4.72 Å.

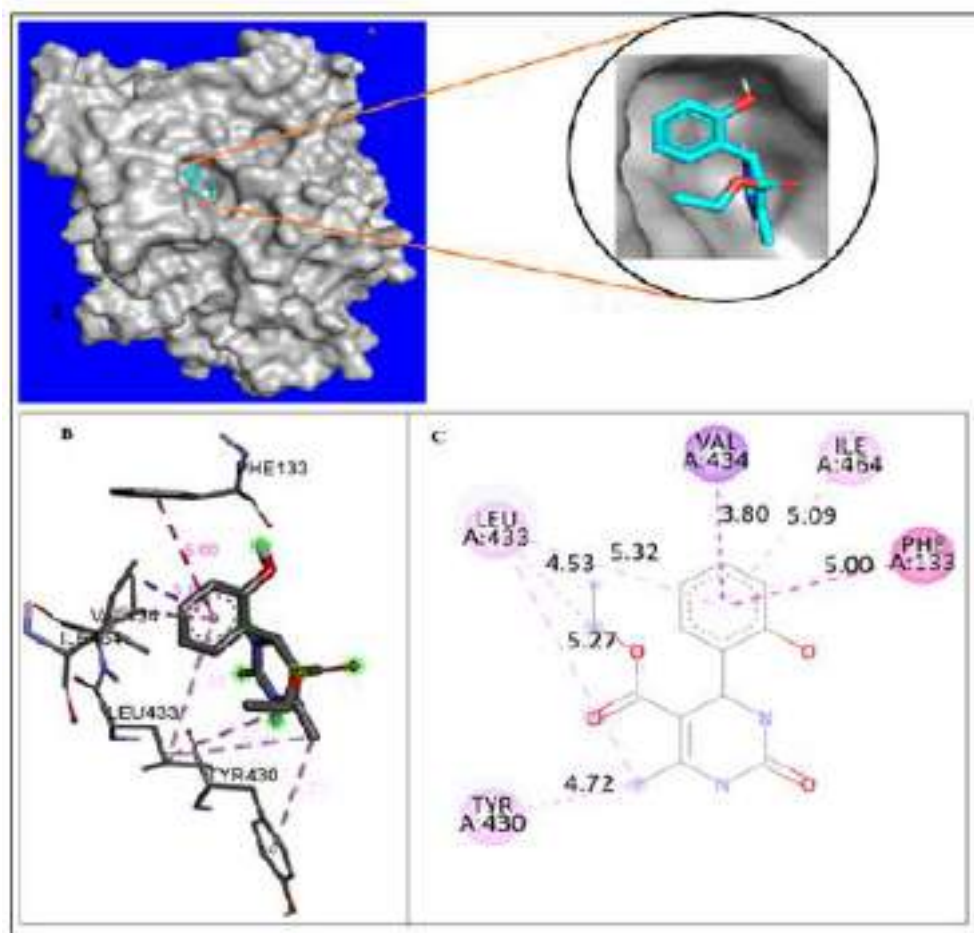


Fig 4.B.8. Visualisation of docking results of ligand DP-1 within a receptor site in the protein 3DH4: (A) Optimal binding mode of the protein with DP-1 ligand (Ligand DP-1 shown as blue and green stick model). (B) Amino acid residues involved in different interactions (purple dash lines show π -sigma interactions, dark pink lines show π - π T-shaped interaction, and light pink dash lines show alkyl and π -alkyl interactions). (C) 2D representation of binding interaction of ligand DP-1 with different amino acid residues of the protein 3DH4.

Visualization of the docking results of the ligand DP-2 with the protein receptor 3DH4 revealed that the ligand fits into a pocket region present in the core region of the protein with the highest binding energy (ΔG) value of -7.9 kcal/mol and the predicted inhibitory constant (pK_i) value of 1.23 μ M. The major interactions between the ligand DP-2 and the protein receptor are characterized by four major conventional hydrogen bonding. These hydrogen bonding are i) between C=O group of the amino residue Glu68 and the -NH group of the ligand DP-2 at a distance of 2.37 Å, ii) between the -NH₂ group present in the amino acid Gln68 and the C=O group of the of the DHPM nucleus of the ligand at a distance of 2.46Å, iii) between the -NH₂ group of the amino acid Asn142 and the carbonyl oxygen atom of the -COOEt group present on the DHPM nucleus at a distance of

by two conventional hydrogen bonding between the -NH group of the residue Phe479 and the carbonyl group of the DHPM nucleus of the ligand at a distance of 2.21Å, and between the C=O group of the residue Met477 and the NH group of the ligand DP-3 at a distance of 2.25Å respectively (Fig.4.B.9). Two unfavorable acceptor-acceptor interaction was encountered between the C=O group of the residue Met244 and the carbonyl group of the ligand DP-3 at a distance of 3.00Å and between the C=O group of the residue Lys471 with the oxygen atom present in the phenyl ring of the ligand DP-3 at a distance of 2.89Å. In addition, a π -donor hydrogen bonding interaction was also observed between the -NH group of the residue Met477 and the π -electron of phenyl ring of the ligand DP-3 at a distance of 2.99Å.

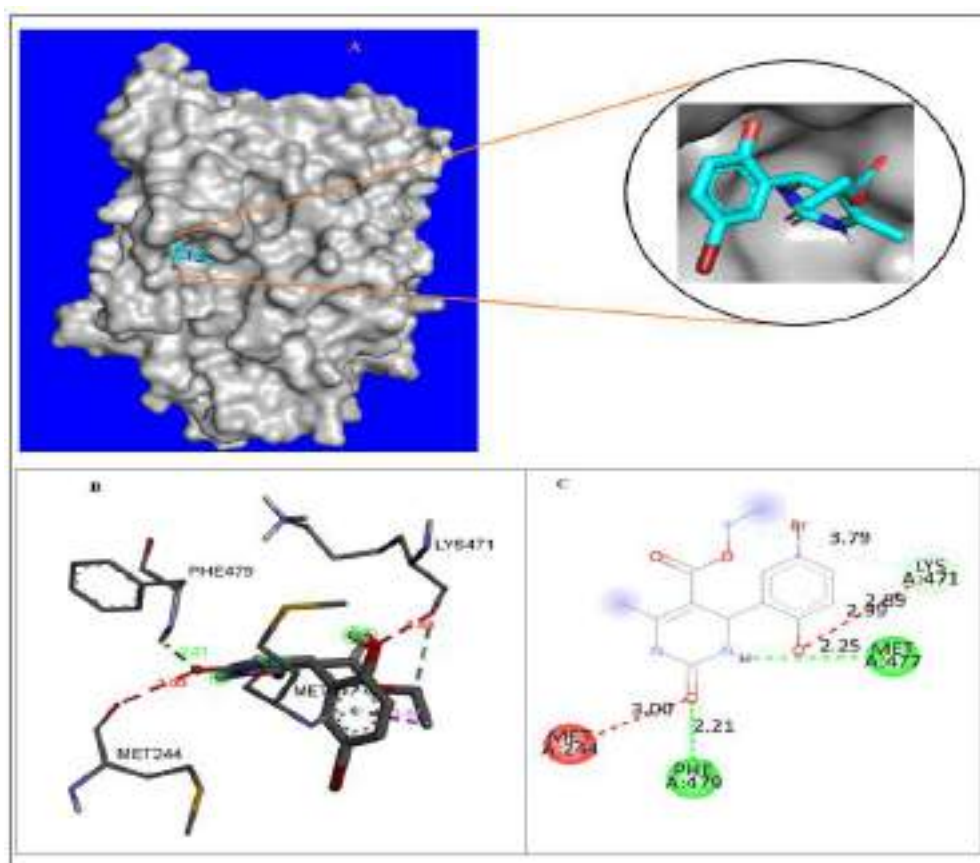


Fig. 4.B.10. Visualisation of docking results of ligand DP-3 within a receptor site in the protein 3DH4: (A) Optimal binding mode of the protein with DP-3 ligand (Ligand DP-3 shown as blue and green stick model). (B) Amino acid residues involved in different interactions (green dash lines show conventional hydrogen bonding interactions, light green dash lines depict carbon hydrogen bonding and π -donor hydrogen bonding interactions, and red dash lines show unfavourable acceptor-acceptor interactions). (C) 2D representation of binding interaction of ligand DP-3 with different amino acid residues of the protein 3DH4.

4.B.2.3 In silico Pharmacokinetic analysis of DP-1 to DP-3

The pharmacokinetic properties like absorption, distribution, metabolism, excretion and toxicity (ADMET) are fundamental properties in determining the drug likeness of any compounds prior to its clinical and animal studies. Therefore, ADMET property of the studied compounds plays an important role in categorizing them as a drug candidate as well as their activity inside the body⁶⁷. The ADMET parameters provide useful information about the concentrations of the drug in the different parts of the body with respect to time⁶⁸. ADMET properties such as gastrointestinal absorption (GI), water solule capability (Log s), lipophilicity (Log Po/W), CYP1A2 inhibitor and Blood-Brain Barrier (BBB) are fundamentally important for any studied compounds to be considered them as a drug candidate⁶⁹. Therefore, the pharmacokinetic properties of the selected 2, 4, 5-triarylimidazole derivatives (IM-1 to IM-6) have been computed with the help of computer aided online SwissADME database (<http://www.swissadme.ch>) and the result of the pharmacokinetic properties along with the Lipinski's property are listed in Table 4.B.8

From the table it is evident that all the studied compounds (DP-1 to DP-3) with bioavailability score in the range of 55% have lipophilicity value (Log Po/W) in the range 1.14-1.79 and has good gastrointestinal absorption. The high and positive value of lipophilicity (LogPo/w) for the studied compounds indicated that the compounds are more lipophilic and these compounds could easily pass through the lipid bilayer of most cellular membrane. From the solubility (Log S) values of the studied compounds which falls in the range of -2.15 to -3.07 it can be said that all the studied compounds are soluble in water. However, the studied compounds do not have any BBB and CYP1A2 properties. It can also be clearly seen that all these compounds have no violations of Lipinski's rule and can be qualified as a potential candidate for a drug.

Table. 4.B.8. Lipinski's properties and pharmacokinetic properties (ADME) of studied compounds DP-1 to DP-3

COMPOUNDS			
Properties	DP-1	DP-2	DP-3
Molecular weight (gm/mole)	276.29	310.73	355.18
Rotatable bonds	4	4	4
H-bond acceptor	4	4	4
H-bond donor	3	3	3
Violations	0	0	0
Log Po/W	1.14	1.71	1.79
Log S	-2.15(S)	-2.75(S)	-3.07
GI	High	High	High
BBB	No	No	No
CYP1A2	No	No	No
Bioavailability Score	0.55	0.55	0.55
Topological Surface Area (A²)	87.66	87.66	87.66

*MS: Moderately soluble, PS: Partially soluble, BBB: Blood-Brain Barrier, CYP: Cytochrome P450, GI: Gastrointestinal absorption

4. B.2.4 Computational details

4.B.2.4.1 DFT study

All Quantum Mechanical calculations were carried out on a hp-Z640 desktop P.C. with an Intel Xeon processor (Specifications: E5-2630 V4 @ 220GHz) using Gaussian 16 W package. Density functional theory (DFT) with Becke's (B)three parameter hybrid model, Lee, Yang and Parr's (LYP) using 631G+(d,2p) basis set has been employed to optimize the geometry of the 3,4-dihydropyrimidin-(2H)-one derivatives (DP-1 to DP-3).

A set of theoretical calculations of selected compounds (DP-1 to DP-3) were performed with Gaussian 16W, Revision A.03 programme package using B3LYP/631G+(d,2p) basis sets to optimize geometry and minimize energy for faster and accurate calculations. With the optimized geometry, theoretical Raman and IR spectra were also calculated from the so chosen basis set. From the optimized geometry, the energy of HOMO and LUMO molecular orbitals along with the energy of HOMO-LUMO gap has also been measured. For analyzing the result of the theoretical calculations, a visual representation was obtained by Gauss View program6 and it has been used to construct the molecular electrostatic

potential surface (MESP) as well as the shape of HOMO and LUMO molecular orbitals. Also, nonlinear Optical property (NLO) of the selected 3,4-dihydropyrimidin-(2H)-one derivatives have also been calculated taking urea as a reference NLO material.

4.B.2.4.2 Preparation of Protein and ligand for docking Study

The X-ray crystallographic structures of phosphorylated insulin receptor tyrosine kinase protein (PDB 3DH4) has been downloaded from the Protein Data Bank (PDB) (<http://www.pdb.org>) database. Graphical User Interface program “Auto Dock Tools (ADT) 1.5.6” from Molecular Graphics Laboratory (MGL) developed by Scripps Research Institute has been used for the preparation of protein for docking study⁶⁶. Input file of receptor protein for the blind docking study were created by taking specific chain (Chain A) of the protein (3DH4). In a typical receptor protein preparation, water molecules and hetero atoms along with the co-crystallized ligands in PDB crystal structure was removed and subsequently, the receptor. pdbqt file has been prepared by adding polar hydrogen atoms and Kollman united atom charges^{62,65}. The three-dimensional (3D) structures of ligands (DP-1 to DP-3) were drawn using Chemsketch (ACD/Structure Elucidator, version 12.01, Advanced Chemistry Development, Inc., Toronto, Canada, 2014, <http://www.acdlabs.com>) and geometry optimization of the ligands (DP-1 to DP-3) were carried out using MM2 program incorporated in Chem. Draw Ultra 8.0 and further optimization of geometry of each molecule were carried out with the MOPAC 6 package using the semi-empirical AM1 Hamiltonian⁷⁰. The input .pdbqt file of the ligands was generated using Auto Dock Tools (ADT). As the ligand molecules (DP-1 to DP-3) were non peptides, therefore, Gasteiger charge was assigned and then non-polar hydrogen was merged.

4.B.2.4.3 Molecular docking study using Autodock vina

All molecular docking calculations of the studied ligands (DP-1 to DP-3) with protein 3DH4 were carried out in the AutoDock Vina programme 1.1.2 developed by Scripps Research institute⁷¹⁻⁷² and the results of the docking study and the intermolecular interactions between receptors protein and the ligand molecules were analyzed using BIOVIA Discovery Studio 2020 (DS), version 20.1.0.0 (Dassault Systèmes BIOVIA, Discovery Studio Modeling Environment, Release 2017, San Diego: Dassault Systèmes, 2016) and Edu pymol version 1.7.4.4⁷². The three-dimensional (3D) affinity (grid) maps and electrostatic a grid boxes of 80×80×80 Å grid points and grid centre (X, Y, Z) of 28.108, -43.008, 59.313 with a spacing of 1.00 Å generated by AutoGrid auxiliary program for each of the receptor protein for blind docking were generated to cover the entire active site of the receptor protein in order to eliminate biasness arising during the docking simulation⁷³. Lamarckian genetic algorithm and a standard protocol with default setting of other run parameters were used for docking simulation. For each docking experiments, several runs were performed by the program with one predicted binding mode with each run. All the torsions were allowed to rotate. The predicted

inhibitory constant (**pK_i**) has been calculated using the following standardized equation⁷⁴

$$pK_i = 10^{\frac{\text{Binding Energy Score}}{1.336}}$$

4.B.2.4.4 Pharmacokinetic study

The pharmacokinetic properties like absorption, distribution, metabolism, excretion and toxicity (ADMET) of the compounds (IM-1 to IM-6) have been studied using the computer aided online SwissADME database (<http://www.swissadme.ch>)

4.B.3 References

- (1) P. Biginelli., *Gazzetta Chimica Italiana*, **1893**, 23 (1), 360–413.
- (2) I. S. Zorkun, S. Saraç, S. Çelebi, K. Erol., *Bioorganic & Medicinal Chemistry*, **2006**, 14 (24), 8582–8589.
- (3) K. S. Atwal, G. C. Rovnyak, B. C. O'Reilly, J. Schwartz., *Journal of Organic Chemistry*, **1989**, 54 (25), 5898–5907.
- (4) Z. Maliga, T. M. Kapoor, T. J. Mitchison., *Chemistry & Biology*, **2002**, 9 (9), 989–996.
- (5) S. DeBonis, J. P. Simorre, I. Crevel, L. Lebeau, D. A. Skoufias, A. Blanzzy, C. Ebel, P. Gans, R. Cross, D. D. Hackney, R. H. Wade, F. Kozielski., *Biochemistry*, **2003**, 42 (2), 338–349.
- (6) K. S. Atwal, B. N. Swanson, S. E. Unger, D. M. Floyd, S. Moreland, A. Hedberg, B. C. O'Reilly., *Journal of Medicinal Chemistry*, **1991**, 34 (2), 806–811.
- (7) M. Brands, R. Endermann, R. Gahlmann, J. Krüger, S. Raddatz., *Bioorganic & Medicinal Chemistry Letters*, **2003**, 13 (2), 241–245.
- (8) M. M. Ghorab, S. M. Abdel-Gawad, M. S. A. El-Gaby., *Il Farmaco*, **2000**, 55 (4), 249–255.
- (9) C. Oliver Kappe, W. M. F. Fabian, M. A. Semones., *Tetrahedron*, **1997**, 53 (8), 2803–2816.
- (10) A. D. Patil, N. V. Kumar, W. C. Kokke, M. F. Bean, A. J. Freyer, C. de Brosse, S. Mai, A. Trunch, D. J. Faulkner, B. Carte, A. L. Breen, R. P. Hertzberg, R. K. Johnson, J. W. Westley, B. C. M. Potts., *Journal of Organic Chemistry*, **1995**, 60 (5), 1182–1188.
- (11) S. K. Sam, S. C. Bo, H. L. Jae, K. L. Ki, H. L. Tae, H. K. Young, H. Shin., *Synlett*, **2009**, 2009 (4), 599–602.
- (12) K. Yamamoto, Y. G. Chen, F. G. Buono., *Organic Letters*, **2005**, 7 (21), 4673–4676.
- (13) X. Wang, Z. Quan, Z. Zhang., *Tetrahedron*, **2007**, 63 (34), 8227–8233.
- (14) X.-C. Wang, Z.-J. Quan, Z. Zhang, Y.-J. Liu, P.-Y. Ji., *Letters in Organic Chemistry*, **2007**, 4, 370–373.
- (15) R. Pérez, T. Beryozkina, O. I. Zbruyev, W. Haas, C. O. Kappe., *Journal of Combinatorial Chemistry*, **2002**, 4 (5), 501–510.
- (16) A. Lengar, C. O. Kappe., *Organic Letters*, **2004**, 6 (5), 771–774.

- (17) B. Khanetsky, D. Dallinger, C. O. Kappe., *Journal of Combinatorial Chemistry*, **2004**, 6 (6), 884–892.
- (18) A. D. Bochevarov, M. A. Watson, J. R. Greenwood, D. M. Philipp., *Journal of Chemical Theory and Computation*, **2016**, 12 (12), 6001–6019.
- (19) M. Mutailipu, Z. Xie, X. Su, M. Zhang, Y. Wang, Z. Yang, M. R. S. A. Janjua, S. Pan., *J Am Chem Soc*, **2017**, 139 (50), 18397–18405.
- (20) A. K. Sharma, W. M. C. Sameera, M. Jin, L. Adak, C. Okuzono, T. Iwamoto, M. Kato, M. Nakamura, K. Morokuma., *J Am Chem Soc*, **2017**, 139 (45), 16117–16125.
- (21) N. D. Yilmazer, M. Korth., *Journal of Physical Chemistry B*, **2013**, 117 (27), 8075–8084.
- (22) M. Evecen, H. Tanak., *Materials Science- Poland*, **2016**, 34 (4), 886–904.
- (23) X. Ma, D. Chang, C. Zhao, R. Li, X. Huang, Z. Zeng, X. Huang, Y. Jia., *Journal of Materials Chemistry C*, **2018**, 6 (48), 13241–13249.
- (24) S. Naseem, M. Khalid, M. N. Tahir, M. A. Halim, A. A. C. Braga, M. M. Naseer, Z. Shafiq., *Journal of Molecular Structure*, **2017**, 1143, 235–244.
- (25) M. Zheng, X. Liu, Y. Xu, H. Li, C. Luo, H. Jiang., *Trends in Pharmacological Sciences*, **2013**, 34 (10), 549–559.
- (26) H. J. Huang, H. W. Yu, C. Y. Chen, C. H. Hsu, H. Y. Chen, K. J. Lee, F. J. Tsai, C. Y. C. Chen., *J Taiwan Inst Chem Eng*, **2010**, 41 (6), 623–635.
- (27) A. Daina, M. C. Blatter, V. Baillie Gerritsen, P. M. Palagi, D. Marek, I. Xenarios, T. Schwede, O. Michielin, V. Zoete., *Journal of Chemical Education*, **2017**, 94 (3), 335–344.
- (28) M. Xiang, Y. Cao, W. Fan, L. Chen, Y. Mo., *Combinatorial Chemistry & High Throughput Screening*, **2012**, 15 (4), 328–337.
- (29) A. B. Olokoba, O. A. Obateru, L. B. Olokoba., *Oman Medical Journal*, **2012**, 27 (4), 269–273.
- (30) A. Maitra, A. K. Abbas., In *Robbins & Cotran Pathologic Basis of Disease (Chapter 24 - Endocrine System)*; Kumar, V., Abbas, A. K., Fausto, N., Aster, J. C., Eds.; Saunders: Philadelphia, **2005**; pp 1156–1226.
- (31) E. C. Chao, R. R. Henry., *Nature Reviews Drug Discovery*, **2010**, 9 (7), 551–559.
- (32) S. Vorberg, I. Koch, C. Buning., *Journal of Cheminformatics*, **2012**, 4 (S1), P41.
- (33) S. Faham, A. Watanabe, G. M. Besserer, D. Cascio, A. Specht, B. A. Hirayama, E. M. Wright, J. Abramson., *Science (1979)*, **2008**, 321 (5890), 810–814.

- (34) J. J. Marín-Peñalver, I. Martín-Timón, C. Sevillano-Collantes, F. J. del Cañizo-Gómez., *World Journal of Diabetes*, **2016**, 7 (17), 395.
- (35) I. D. Kuntz., *Science (1979)*, **1992**, 257 (5073), 1078–1082.
- (36) J. Drews., *Science*, **2000**, 287 (5460), 1960–1964.
- (37) I. Muegge, M. Rarey., In *Reviews in Computational Chemistry (Chap 1 - Small Molecule Docking and Scoring)*; Lipkowitz, K. B., Boyd, D. B., Eds.; John Wiley & Sons, Ltd: New York, **2001**; Vol. 17, pp 1–60.
- (38) S. F. Sousa, P. A. Fernandes, M. J. Ramos., *Proteins*, **2006**, 65 (1), 15–26.
- (39) A. D. Becke., *The Journal of Chemical Physics*, **1993**, 98 (7), 5648–5652.
- (40) C. Lee, W. Yang, R. G. Parr., *Physical Review B*, **1988**, 37 (2), 785–789.
- (41) M. J. Frisch, G. W. Trucks, H. B. Schlegel, G. E. Scuseria, M. A. Robb, J. R. Cheeseman, G. Scalmani, V. Barone, G. A. Petersson, H. Nakatsuji, X. Li, M. Caricato, A. v Marenich, J. Bloino, B. G. Janesko, R. Gomperts, B. Mennucci, H. P. Hratchian, J. v Ortiz, A. F. Izmaylov, J. L. Sonnenberg, D. Williams-Young, F. Ding, F. Lipparini, F. Egidi, J. Goings, B. Peng, A. Petrone, T. Henderson, D. Ranasinghe, V. G. Zakrzewski, J. Gao, N. Rega, G. Zheng, W. Liang, M. Hada, M. Ehara, K. Toyota, R. Fukuda, J. Hasegawa, M. Ishida, T. Nakajima, Y. Honda, O. Kitao, H. Nakai, T. Vreven, K. Throssell, J. A. Montgomery Jr., J. E. Peralta, F. Ogliaro, M. J. Bearpark, J. J. Heyd, E. N. Brothers, K. N. Kudin, V. N. Staroverov, T. A. Keith, R. Kobayashi, J. Normand, K. Raghavachari, A. P. Rendell, J. C. Burant, S. S. Iyengar, J. Tomasi, M. Cossi, J. M. Millam, M. Klene, C. Adamo, R. Cammi, J. W. Ochterski, R. L. Martin, K. Morokuma, O. Farkas, J. B. Foresman, D. J. Fox., *Gaussian, Inc., Wallingford CT, Gaussian 16 Revision C.01*, **2016**.
- (42) R. Dennington, T. A. Keith, J. M. Millam., *GaussView Version 6, Semichem Inc., Shawnee Mission, KS*, **2016**.
- (43) P. Sykes., *A Guidebook to Mechanism in Organic Chemistry*, 6th ed.; Pearson Education: New Delhi, India, **2004**.
- (44) K. B. Benzon, H. T. Varghese, C. Y. Panicker, K. Pradhan, B. K. Tiwary, A. K. Nanda, C. van Alsenoy., *Spectrochimica Acta Part A: Molecular and Biomolecular Spectroscopy*, **2015**, 151, 965–979.
- (45) S. W. Xia, X. Xu, Y.-L. Sun, Y.-H. Fan, C.-F. Bi, D. M. Zhang, L.-R. Yang., *Chinese Journal of Structural Chemistry*, **2006**, 25 (2), 197–203.
- (46) M. Snehathatha, C. Ravikumar, I. Hubert Joe, N. Sekar, V. S. Jayakumar., *Spectrochimica Acta Part A: Molecular and Biomolecular Spectroscopy*, **2009**, 72 (3), 654–662.

- (47) T. A. Koopmans., *Physica*, **1934**, *1* (1–6), 104–113.
- (48) R. G. Parr, L. V. Szentpály, S. Liu., *J Am Chem Soc*, **1999**, *121* (9), 1922–1924.
- (49) R. G. Parr, R. G. Pearson., *J Am Chem Soc*, **1983**, *105* (26), 7512–7516.
- (50) R. G. Pearson., *Journal of Chemical Sciences*, **2005**, *117* (5), 369–377.
- (51) S. Mandal, D. K. Poria, D. K. Seth, P. S. Ray, P. Gupta., *Polyhedron*, **2014**, *73*, 12–21.
- (52) P. Jaramillo, P. Pérez, R. Contreras, W. Tiznado, P. Fuentealba., *Journal of Physical Chemistry A*, **2006**, *110* (26), 8181–8187.
- (53) N. P. G. Roeges., *A Guide to the Complete Interpretation of Infrared Spectra of Organic Structures*; John Wiley and Sons Inc.: New York, **1994**.
- (54) B. C. Smith., *Infrared Spectral Interpretation, A Systematic Approach*, 1st ed.; CRC Press: Washington, DC, **1999**; Vol. 2.
- (55) P. Politzer, D. G. Truhlar., *Chemical Applications of Atomic and Molecular Electrostatic Potentials*; Plenum Press: New York, **1981**.
- (56) E. Scrocco, J. Tomasi., *Advances in Quantum Chemistry*, **1978**, *11* (C), 115–193.
- (57) P. Politzer, J. S. Murray., In *Theoretical Biochemistry and Molecular Biophysics: A Comprehensive Survey, Protein*; Beveridge, D. L., Lavery, R., Eds.; Adenine Press: Schenectady, New York, **1991**.
- (58) E. Scrocco, J. Tomasi., *Topics in Current Chemistry*, **1973**, *42*, 95–170.
- (59) *Principles and Applications of Nonlinear Optical Materials*, 1st ed.; Munn, R. W., Ironside, C. N., Eds.; Springer Dordrecht: Netherlands, **1993**.
- (60) A. Migalska-Zalas, K. el Korchi, T. Chtouki., *Optical and Quantum Electronics*, **2018**, *50(11)* (Article no. 389), 1–10.
- (61) A. P. Caricato, W. Ge, A. D. Stiff-Roberts., In *Advances in the Application of Lasers in Materials Science, (Chap 10 - UV- and RIR-MAPLE: Fundamentals and applications)*; Ossi, P. M., Ed.; Springer Verlag, **2018**; pp 275–308.
- (62) L. Ferreira, R. dos Santos, G. Oliva, A. Andricopulo., *Molecules*, **2015**, *20* (7), 13384–13421.
- (63) (Editorial) Eric C. Westman., *Frontiers in Nutrition*, **2021**, *8* (827990), 1–5.
- (64) C. Hale, M. Wang., *Mini Reviews in Medicinal Chemistry*, **2008**, *8* (7), 702–710.
- (65) X.-Y. Meng, H.-X. Zhang, M. Mezei, M. Cui., *Current Computer-Aided Drug Design*, **2011**, *7* (2), 146–157.

- (66) R. Huey, G. M. Morris., *The Scripps Research Institute, USA*, **2008**, 8, 54–56.
- (67) S. Hari., *Journal of Applied Pharmaceutical Science*, **2019**, 9 (7), 18–26.
- (68) K. Boussery, F. M. Belpaire, J. van de Voorde., In *The Practice of Medicinal Chemistry*; Wermuth, C. G., Ed.; Elsevier Science, **2008**; pp 635–654.
- (69) F. Ntie-Kang, L. L. Lifongo, J. A. Mbah, L. C. Owono Owono, E. Megnassan, L. M. Mbaze, P. N. Judson, W. Sippl, S. M. N. Efange., *In Silico Pharmacology*, **2013**, 1(1) (Article 12), 1–11.
- (70) K. Ohtawara, H. Teramae., *Chemical Physics Letters*, **2004**, 390 (1–3), 84–88.
- (71) J. Eberhardt, D. Santos-Martins, A. F. Tillack, S. Forli., *Journal of Chemical Information and Modeling*, **2021**, 61 (8), 3891–3898.
- (72) O. Trott, A. J. Olson., *Journal of Computational Chemistry*, **2010**, 31 (2), 455–461.
- (73) G. M. Morris, D. S. Goodsell, R. S. Halliday, R. Huey, W. E. Hart, R. K. Belew, A. J. Olson., *Journal of Computational Chemistry*, **1998**, 19 (14), 1639–1662.
- (74) M. A. Alamri, M. Tahir ul Qamar, M. U. Mirza, R. Bhadane, S. M. Alqahtani, I. Muneer, M. Froeyen, O. M. H. Salo-Ahen., *Journal of Biomolecular Structure and Dynamics*, **2021**, 39 (13), 4936–4948.